Couple stress in the vertex model of cellular monolayers

OEJ & CR

March 2, 2022

Abstract

The vertex model is widely used to simulate the mechanical properties of confluent epithelia and other multicellular tissues. This inherently discrete framework allows a Cauchy stress to be attributed to each cell, and its symmetric component has been widely reported, at least for planar monolayers. Here we consider the stress attributed to the neighbourhood of each tricellular junction, deriving in particular its leading-order antisymmetric component and the associated distribution of couple stress, which can be used to characterise the degree to which individual cells experience (and resist) in-plane bending deformations. We derive the associated discrete scalar potentials (analogues of Airy and Mindlin stress functions), *which we use to visualise stress patterns in monolayers.*

1 Introduction

The vertex model is a powerful tool for describing the mechanics of spatially heterogeneous multicellular tissues [1, 2, 3, 4, 5]. A confluent planar epithelium, for example, is represented as polygons tiling a plane. A mechanical strain energy is attributed to each cell that is a function of geometric invariants (such as the cell's area and perimeter) and the total energy of the monolayer is minimised, at a rate defined via a model of viscous dissipation, by varying vertex locations, potentially allowing for cell neighbour exchanges (so-called T1 transitions). A force balance at each vertex is used to evolve the system to equilibrium; elastic forces are defined by taking the first variation of each cell's mechanical energy with respect to vertex displacements. The changes of a cell's area and perimeter arising from small displacements of its vertices can thereby be used to define the mechanical (Cauchy) stress attributed to each cell. The model predicts a symmetric Cauchy stress tensor associated with each cell [6, 7] that aligns with cell shape [8] and allows viscoelastic moduli for bulk and shear deformations to be evaluated [9, 10]. Less attention has been paid to the Cauchy stress defined over the network that is topologically dual to cellular polygons, namely the triangulation connecting adjacent cell centres. The stress attributed to each triangle describes the mechanical environment in the neighbourhood of the tricellular junction lying within the triangle. This stress field is of interest given the role of tricellular junctions as potential sensors of cell shape and mechanical stress [11, 12, 13, 14, 15].

From a multiscale modelling perspective, the vertex model is also of interest as a bridge between descriptions of discrete cells in a tissue and a continuum description of the tissue's mechanical properties. In two-dimensional (2D) continuum mechanics, it is often convenient to express the Cauchy stress in terms of a scalar potential, the Airy stress function [16]. However in seeking to construct the discrete analogue of the Airy stress function, we found [17] that the requirement for both forms of the Cauchy stress (that defined over cells, and that defined over tricellular junctions) to be symmetric places severe geometric constraints on cell shape, specifically that cell edges should be orthogonal to links between cell centres and that each vertex should lie at the orthocentre of the triangle formed by its immediate neighbours. These constraints are not met in typical simulations (nor, indeed, in real monolayers). This discrepancy can be explained in part by noting that while forces balance at vertices in the normal implementation of the vertex model, torque balance is not enforced. Here we consider how the discrepancy can be accommodated by relaxing the requirement for all Cauchy stresses to be symmetric, by incorporating couple stresses within the constitutive framework, which we evaluate for a standard implementation of the vertex model. In effect, the finite size of cells endows the monolayer with features not normally found in homogeneous materials.

The Cauchy stress attributed to a cell (which hereafter we call the force stress, evaluated as the first spatial moment of the forces acting over a cell) can be partitioned into an isotropic component (defining an effective cell pressure) and a deviatoric component (describing the shear stress experienced by each cell) [8]. Analogous quantities can be attributed to the triangles bounding tricellular junctions, having vertices at cell centres. The couple stress provides an additional measure of the stress arising from in-plane bending deformations. Using a standard version of the vertex model, we show here how the degree to which a cell is 'bent out of shape' can be evaluated in simple geometric terms (by considering second-order spatial gradients of a virtual tissue deformation), and demonstrate that while individual cells experience zero torque, a couple can be exerted around tricellular junctions generated by pressure differences that create moments acting across adjacent cell edges.

Our calculations are facilitated through use of tools of discrete calculus [18]. In particular, incidence matrices explicitly capture topological relationships between cell vertices, edges and faces and enable the primal network of polygonal cells to be related directly to the dual triangulation connecting adjacent cell centres. Incidence matrices also provide the building blocks of the discrete differential operators needed to represent stresses using vector and scalar potentials. Unlike the three operators needed for normal continuum mechanics (grad, div and curl), we find that up to 16 different operators (4 grads, 4 divs and 8 curls) are required in two spatial dimensions, in the general instance when links between cell centres are not orthogonal to cell edges. These operators provide representations of spatially-2D vectors in terms of scalar potentials, via Helmholtz decomposition. For 2D continuum elasticity, two potentials suffice for simply-connected domains (the Airy stress function, plus an additional stress function defined by Mindlin for couple-stress materials [19, 20]). For discrete networks of cells, we find that up to eight potentials typically emerge, four defined over the network of cells, and four over the dual triangulation, although these reduce in number when edges and links are orthogonal. We consider how potentials enable *visualisation of stress patterns* across a monolayer.

We briefly review continuous couple-stress materials in 2D in Appendix A, following [20]. Key points to highlight are: (i) the Cauchy stress $\boldsymbol{\sigma}$ and couple stress vector $\boldsymbol{\mu}$ can be written in terms of Airy and Mindlin stress functions ψ and Ψ in the the form

$$\boldsymbol{\sigma} = \mathrm{curl} \otimes (\mathrm{curl}\, \psi - \mathrm{grad}\, \Psi), \quad \boldsymbol{\mu} = -\mathrm{curl}\, \Psi, \tag{1}$$

automatically satisfying the force balance $\mathrm{div}\, \boldsymbol{\sigma} = \mathbf{0}$, a torque balance relating the antisymmetric component of $\boldsymbol{\sigma}$ to $\mathrm{curl}\, \boldsymbol{\mu}$ and a compatibility condition (derived from a constitutive assumption) $\mathrm{div}\, \boldsymbol{\mu} = 0$; (ii) the vector potential $\mathrm{curl}\, \psi - \mathrm{grad}\, \Psi$ is here expressed using a Helmholtz decomposition in terms of the two scalar potentials ψ and Ψ; and (iii) in the principle of virtual work, the strain $\frac{1}{2}(\nabla \mathbf{u} + \nabla \mathbf{u}^\top)$ of a small-amplitude deformation $\mathbf{u}(\mathbf{x})$ is energy-conjugate to $\boldsymbol{\sigma}$ while $\frac{1}{2}(\nabla^2 \mathbf{u} - \nabla(\nabla \cdot \mathbf{u})) = -2\boldsymbol{\kappa}$ (a strain gradient), where $\boldsymbol{\kappa}$ is the so-called curvature, is energy-conjugate to $\boldsymbol{\mu}$. We seek discrete analogues of these relationships below (disregarding the compatibility condition $\mathrm{div}\, \boldsymbol{\mu} = 0$, as we make an alternative constitutive assumption), starting by describing the nature of Helmholtz decompositions over a discrete cellular network and its dual triangulation. Key quantities and results are summarised in Sec. 2, with details provided in Appendix B. In particular, we identify four Laplacians associated with the 16 operators, through which scalar potentials can (in principle) be derived to describe any vector field defined over the cell network. We then recall how stresses in a vertex model can be expressed in terms of a force potential (in Sec. 3.1, following [17]) and discuss the underlying scalar potentials (Sec. 3.2). Using a standard constitutive model, we derive in Sec. 4 the couple stress vector. Results are *illustrated by computations in Sec. 5* and discussed in Sec. 6.

2 Discrete calculus for a cellular monolayer

2.1 Cell topology

We consider an isolated cellular monolayer occupying a simply-connected domain on the Euclidean plane. Adopting notation used in [17], vertices, edges and faces of the (primal) cell network are labelled by k, j and i respectively (Figure 1), where $i = 1, \ldots, N_c$, $j = 1, \ldots, N_e$ and $k = 1, \ldots, N_v$. Orientations are assigned to each object and (signed) incidence matrices A_{jk} $[B_{ij}]$ then define topological relationships between edges and

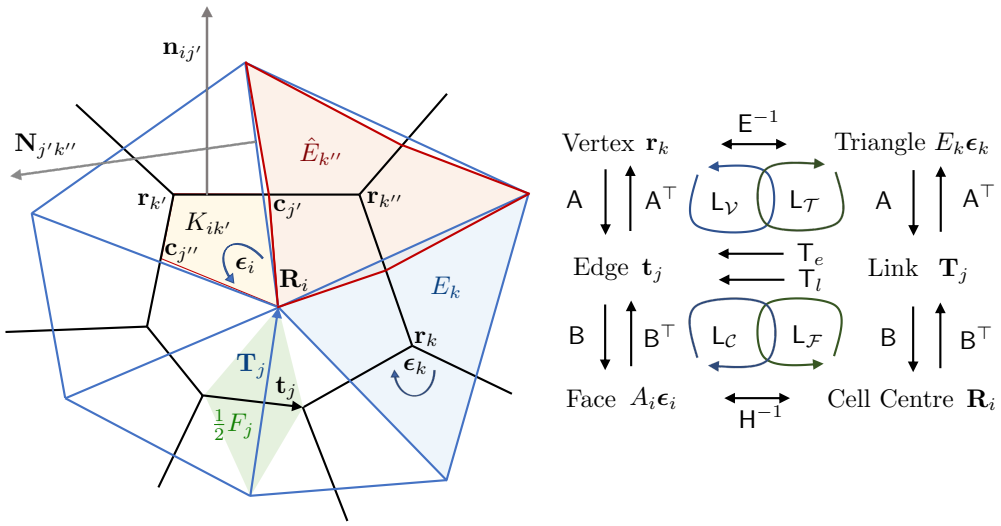

Figure 1: Left: sketch defining geometric objects, their orientations and their labels. Black lines denote cell edges, passing through vertices $\mathbf{r}_k$, $\mathbf{r}_{k'}$ and $\mathbf{r}_{k''}$; blue lines denote links between cell centres, including $\mathbf{R}_i$. Yellow: the kite of cell i at vertex k' with area $K_{ik'}$, with two of its vertices at edge centroids $\mathbf{c}_j$ and $\mathbf{c}_{j''}$. Green: the trapezium with area $\frac{1}{2}F_j$ spanned by edge $\mathbf{t}_j$ and link $\mathbf{T}_j$ (orientations of other edges and links are not shown). Blue: the triangle surrounding vertex k with area E_k. Orange: the tristar (made from three kites) surrounding vertex k'' with area $\hat{E}_{k''}$. Edge centroid $\mathbf{c}_{j'}$ sits on its boundary. Also shown are the outward normals $\mathbf{n}_{ij'}$ to cell i at edge j', and $\mathbf{N}_{j'k''}$, to triangle k'' at edge j'. Right: a diagram indicating how incidence matrices A and B map between vertices, edges, faces on the primal network, and cell centres, links and triangles on the dual network. Metric matrices E^{-1}, T_e, T_l and H^{-1} map between networks. Loops indicate how the Laplacians $\mathsf{L}_\mathcal{V}$, $\mathsf{L}_\mathcal{T}$, $\mathsf{L}_\mathcal{C}$, $\mathsf{L}_\mathcal{F}$ (see (7)) are constructed.

vertices [faces and edges]. (Thus $A_{jk} = 1$ if edge j points into vertex k, $A_{jk} = -1$ if edge j points out of vertex k; and $A_{jk} = 0$ otherwise; $B_{ij} = 1$ if edge j neighbours cell i and has congruent orientation; $B_{ij} = -1$ if edge j neighbours cell i but has opposite orientation; and $B_{ij} = 0$ otherwise.) A and B also specify topological relationships between cell centres (assumed here to be cell vertex centroids), links between cell centres and triangular faces of the dual network. Vertices within the interior of a monolayer are assumed to neighbour three cells: vertex/face neighbours are identified by the adjacency matrix $\mathsf{C} = \frac{1}{2}\overline{\mathsf{B}}\,\overline{\mathsf{A}}$, where $\overline{\mathsf{A}}$ and $\overline{\mathsf{B}}$ are unsigned incidence matrices ($\overline{A}_{jk} = |A_{jk}|$, $\overline{B}_{ij} = |B_{ij}|$). Neighbour exchanges are not considered in the present study, so that incidence matrices remain fixed. We also identify centroids of each edge: each cell can then be partitioned into kites (labelled by ik, see Figure 1). Taking the cell network to be primal, the dual network that we will consider is the triangulation defined by cell centroids. In general, links between cell centroids in this network do not pass through edge centroids, except for those in cells at the periphery of the monolayer; thus the faces of the dual network are internal triangles, or kites within cells at the periphery of the monolayer.

A dual network can be constructed allowing the three kites neighbouring each vertex to form a 'tristar' with three vertices at cell centres (Figure 1).

2.2 Cell geometry

We introduce geometric information as follows. Points in the underlying Euclidean plane have position vector $\mathbf{x}$. Where necessary, p, q, r denote subscripts of vectors and tensors, identifying components with respect to a fixed basis in this plane, and a bold font is used to denote vectors with components p, q, r, etc. On the primal network of cells, we define vertices by $\mathbf{r}_k$, edges by $\mathbf{t}_j = \sum_k A_{jk}\mathbf{r}_k$, edge lengths by $t_j = |\mathbf{t}_j|$ and edge centroids by $\mathbf{c}_j = \frac{1}{2}\sum_k \overline{A}_{jk}\mathbf{r}_k$. Thus the non-zero elements of $\mathbf{c}_j^p = \sum_i |\mathbb{1}_i B_{ij}|\mathbf{c}_j$ are the edge centroids around the periphery of the monolayer, where $\mathbb{1}_i = (1, 1, \ldots, 1)$ is the vector (a 2-chain, in the language of discrete

calculus) denoting all cells in the monolayer. The number of edges of cell i is given by $Z_i = \sum_j \overline{B}_{ij}$. We define the centre of cell i as $\mathbf{R}_i = Z_i^{-1} \sum C_{ik}\mathbf{r}_k$. Links on the dual network, triangulating cell centres, are defined by

$$\mathbf{T}_j = \textstyle\sum_i B_{ij}(\mathbf{R}_i - \mathbf{c}_j^p), \tag{2}$$

so that links either connect cell centres or connect centres of border cells to peripheral edge centroids. Orientations of cell faces on the primal network $\boldsymbol{\epsilon}_i$, and triangles (or peripheral kites) on the dual network $\boldsymbol{\epsilon}_k$, are prescribed as $\pm\boldsymbol{\varepsilon}$, where the matrix $\boldsymbol{\varepsilon}$ (the 2D Levi-Civita tensor) represents a clockwise $\pi/2$ rotation. $\boldsymbol{\epsilon}_i$ and $\boldsymbol{\epsilon}_k$ are taken to be independent of i and k respectively and of opposite sense. Orientations of edges $\mathbf{t}_j$ and links $\mathbf{T}_j$ are constrained such that

$$\mathbf{T}_j \cdot \boldsymbol{\epsilon}_i \mathbf{t}_j = \mathbf{t}_j \cdot \boldsymbol{\epsilon}_k \mathbf{T}_j = F_j > 0, \tag{3}$$

where $\frac{1}{2}F_j$ is the area of the trapezium spanned by $\mathbf{t}_j$ and $\mathbf{T}_j$ (for interior edges, Fig. 1) or the area of the triangle spanned by $\mathbf{t}_j$ and $\mathbf{T}_j$ (for peripheral edges). Consistent with typical simulations of the vertex model [17], we allow edges and links to be non-orthogonal.

For cell i, the outward normal to edge j is $\mathbf{n}_{ij} = -\boldsymbol{\epsilon}_i B_{ij}\mathbf{t}_j$. The cell area satisfies

$$\textstyle\sum_j B_{ij}\mathbf{t}_j \otimes \mathbf{c}_j = A_i\boldsymbol{\epsilon}_i, \tag{4}$$

so that $A_i = \frac{1}{2}\sum_j \mathbf{n}_{ij} \cdot \mathbf{c}_j$, and the cell perimeter satisfies $L_i = \sum_j \overline{B}_{ij} t_j$. We define $E_k = \frac{1}{2}A_{jk}A_{j'k}|\mathbf{T}_j \cdot \boldsymbol{\varepsilon}\mathbf{T}_{j'}|$ for $j \neq j'$ as the area of each triangle at interior vertex k, and the area of the adjacent kite if k identifies a peripheral vertex. The outward normal to the triangle connecting adjacent cell centres is $\mathbf{N}_{jk} = -\boldsymbol{\epsilon}_k A_{jk}\mathbf{T}_j$ (Figure 1). The total monolayer area $\mathcal{A}$ can be written

$$\mathcal{A} = \textstyle\sum_i A_i = \sum_j \frac{1}{2}F_j = \sum_k E_k. \tag{5}$$

[*Define E_k as triangle area, distinguish it from tristar area $\hat{E}_k$.*]

To summarise, all topological information is encoded in A and B, while metric information is encoded in edge and link lengths t_j, $T_j = |\mathbf{T}_j|$ and in the areas A_i, E_k and F_j. Using these we define the matrices

$$\mathsf{H} = \mathrm{diag}(A_1, \ldots, A_{N_c}), \quad \mathsf{E} = \mathrm{diag}(E_1, \ldots, E_{N_v}), \quad \mathsf{T}_e = \mathrm{diag}\left(\frac{t_1^2}{F_1}, \ldots, \frac{t_{N_e}^2}{F_{N_e}}\right), \ \mathsf{T}_l = \mathrm{diag}\left(\frac{T_1^2}{F_1}, \ldots, \frac{T_{N_e}^2}{F_{N_e}}\right) \tag{6}$$

with which we can define the square symmetric matrices

$$\mathsf{L}_\mathcal{V} = \mathsf{E}^{-1}\mathsf{A}^\top\mathsf{T}_e^{-1}\mathsf{A}, \quad \mathsf{L}_\mathcal{T} = \mathsf{E}^{-1}\mathsf{A}^\top\mathsf{T}_l\mathsf{A}, \quad \mathsf{L}_\mathcal{C} = \mathsf{H}^{-1}\mathsf{B}\mathsf{T}_l^{-1}\mathsf{B}^\top, \quad \mathsf{L}_\mathcal{F} = \mathsf{H}^{-1}\mathsf{B}\mathsf{T}_e\mathsf{B}^\top. \tag{7}$$

The construction of these operators is illustrated in Figure 1 and explained in more detail below.

2.3 Discrete operators

Variables (so-called co-chains) defined over cells, edges or vertices are written without the i, j, k subscript, so that $\{A\}_i = A_i$, $\{\mathbf{c}\}_j = \mathbf{c}_j$, $\{E\}_k = E_k$, etc. Appendix B describes how discrete analogues of grad, div and curl operators for scalar-valued variables defined on vertices or cell centres, and vector-valued variables defined on edges or links, can be defined. Figure 2 illustrates how the 16 operators act. Explicit expressions for the 8 so-called primary operators are given in Table 1. To summarise briefly, vector-valued cochains defined on edges or links sit in the isomorphic vector spaces $\mathcal{E}$ and $\mathcal{L}$ respectively, which can be partitioned into subspaces $\mathcal{E} = \mathcal{E}^\parallel \oplus \mathcal{E}^\perp$ [or $\mathcal{L} = \mathcal{L}^\parallel \oplus \mathcal{L}^\perp$] of vectors parallel and pependicular to edges [or links]. grad^v and grad^c act on scalars defined at vertices and cell centres (in vector spaces $\mathcal{V}$ and $\mathcal{C}$ respectively), creating vectors in $\mathcal{E}^\parallel$ and $\mathcal{L}^\parallel$ respectively. curl^v and CURL^c are rotated gradients that create vectors that are normal to edges and links respectively (in $\mathcal{E}^\perp$ and $\mathcal{L}^\perp$). div^v and div^c measure fluxes of vectors normal to edges and links, mapping vectors from $\mathcal{E}^\perp$ and $\mathcal{L}^\perp$ to scalars defined over faces and triangles (in spaces $\mathcal{F}$ and $\mathcal{T}$ respectively). CURL^v and curl^c act similarly, but measure fluxes parallel to edges and links. These operators respect the

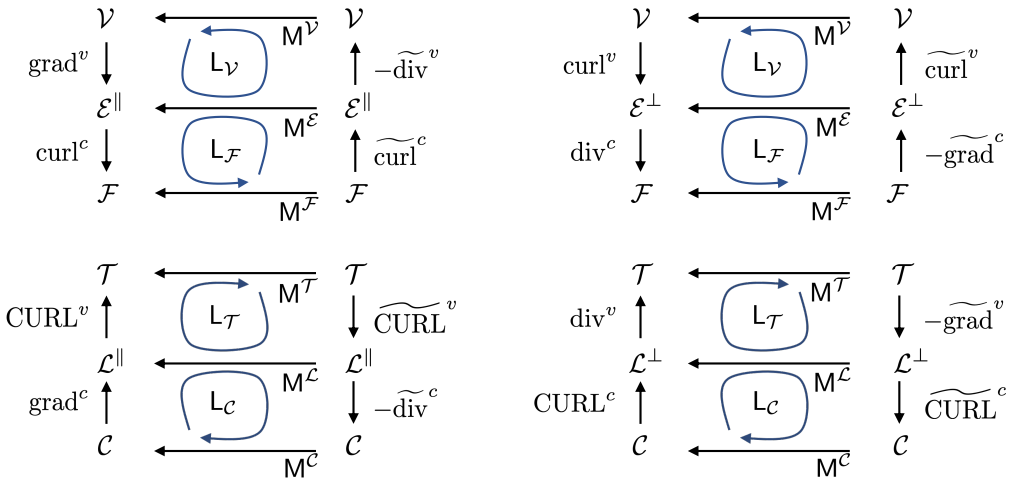

Figure 2: Four commutative diagrams showing operators defined on the primal network (top) and dual network (bottom), involving vectors parallel (left) and perpendicular (right) to edges and links. In each diagram, primary operators run along left-hand vertical arrows. Derived operators, running along right-hand vertical arrows, are adjoint to primary operators under inner products (horizontal arrows) acting on elements of vector spaces $\mathcal{V} \simeq \mathcal{T}$, $\mathcal{E} \simeq \mathcal{L}$, $\mathcal{F} \simeq \mathcal{C}$. Loops show how operators and inner products create scalar Laplacians $\mathsf{L}_{\mathcal{V}}$, $\mathsf{L}_{\mathcal{F}}$, $\mathsf{L}_{\mathcal{T}}$, $\mathsf{L}_{\mathcal{C}}$.

Primary	$\{\mathrm{grad}^v\,\phi\}_j$	$\sum_k A_{jk}(\mathbf{t}_j/t_j^2)\phi_k$	$\{\mathrm{curl}^v\phi\}_j$	$\sum_k \boldsymbol{\epsilon}_k(\mathbf{t}_j/t_j^2)A_{jk}\phi_k$
	$\{\mathrm{curl}^c\,\mathbf{b}\}_i$	$\sum_j B_{ij}\mathbf{t}_j\cdot\mathbf{b}_j/A_i$	$\{\mathrm{div}^c\,\mathbf{b}\}_i$	$-\sum_j B_{ij}(\boldsymbol{\epsilon}_i\mathbf{t}_j)\cdot\mathbf{b}_j/A_i$
	$\{\mathrm{grad}^c\,f\}_j$	$\sum_i B_{ij}(\mathbf{T}_j/T_j^2)f_i$	$\{\mathrm{CURL}^c f\}_j$	$\sum_k \boldsymbol{\epsilon}_i(\mathbf{T}_j/T_j^2)B_{ij}f_i$
	$\{\mathrm{CURL}^v\,\mathbf{b}\}_k$	$\sum_j A_{jk}\mathbf{T}_j\cdot\mathbf{b}_j/E_k$	$\{\mathrm{div}^v\,\mathbf{b}\}_k$	$-\sum_j A_{jk}(\boldsymbol{\epsilon}_k\mathbf{T}_j)\cdot\mathbf{b}_j/E_k$
Derived	$\{\widetilde{\mathrm{grad}}^v\,\phi\}_j$	$\sum_k A_{jk}\boldsymbol{\epsilon}_k(\mathbf{T}_j/F_j)\phi_k$	$\{\widetilde{\mathrm{CURL}}^v\,\phi\}_j$	$\sum_j A_{jk}\mathbf{T}_j\phi_k/F_j$
	$\{\widetilde{\mathrm{CURL}}^c\,\mathbf{b}\}_i$	$\sum_j B_{ij}(F_j/T_j{}^2)(\boldsymbol{\epsilon}_i\mathbf{T}_j)\cdot\mathbf{b}_j/E_k$	$\{\widetilde{\mathrm{div}}^c\,\mathbf{b}\}_i$	$-\sum_j B_{ij}(F_j/T_j^2)\mathbf{T}_j\cdot\mathbf{b}_j/A_i$
	$\{\widetilde{\mathrm{grad}}^c\,f\}_j$	$\sum_i B_{ij}\boldsymbol{\epsilon}_i(\mathbf{t}_j/F_j)f_i$	$\{\widetilde{\mathrm{curl}}^c\,f\}_j$	$\sum_i B_{ij}(\mathbf{t}_j/F_j)f_i$
	$\{\widetilde{\mathrm{curl}}^v\,\mathbf{b}\}_k$	$\sum_j A_{jk}(F_j/t_j^2)(\boldsymbol{\epsilon}_k\mathbf{t}_j)\cdot\mathbf{b}_j/E_k$	$\{\widetilde{\mathrm{div}}^v\,\mathbf{b}\}_k$	$-\sum_j A_{jk}(F_j/t_j^2)\mathbf{t}_j\cdot\mathbf{b}_j/E_k$

Table 1: A summary of the 16 discrete operators, defined in (53, 68), ...

exact relationships $\mathrm{curl}^c\circ\mathrm{grad}^v = 0$, $\mathrm{div}^c\circ\mathrm{curl}^v = 0$ and so on, as summarised in Fig. 2. Superscripts v and c are used to denote objects associated with cells and vertices respectively, and therefore primarily involve B and A respectively.

We note from (4) that $\mathrm{div}^c\,\mathbf{c}_j = 2$ and $\mathrm{curl}^c\,\mathbf{c}_j = 0$. Likewise if $\mathbf{C}_j$ denotes the mid-points of edges of the dual network (so $\mathbf{C}_j = \frac{1}{2}\sum_i \overline{B}_{ij}\mathbf{R}_i$ for internal triangles) then $\mathrm{div}^v\,\mathbf{C}_j = 2$ and $\mathrm{CURL}^v\,\mathbf{C}_j = 0$.

When edges and links are non-orthogonal ($\mathbf{t}_j\cdot\mathbf{T}_j \neq 0$), as we assume to be the case, a further eight so-called derived operators (adjoints under a suitable inner product, denoted with a tilde) must be considered (included in Fig. 2); definitions are given in (61) and (69). Thereby we derive scalar Laplacians $\mathsf{L}_{\mathcal{F}} = -\mathrm{div}^c\circ\widetilde{\mathrm{grad}}^c = \mathrm{curl}^c\circ\widetilde{\mathrm{curl}}^c$ acting on cell faces, and $\mathsf{L}_{\mathcal{V}} = -\widetilde{\mathrm{div}}^v\circ\mathrm{grad}^v = \widetilde{\mathrm{curl}}^v\circ\mathrm{curl}^v$ on vertices, given by (63) and explicitly as

$$\{\mathsf{L}_{\mathcal{F}}\Psi^c\}_i = A_i^{-1}\sum_{j,i'} B_{ij}\frac{t_j^2}{F_j}B_{i'j}\Psi^c_{i'}, \quad \{\mathsf{L}_{\mathcal{V}}\Psi^v\}_k = E_k^{-1}\sum_{j,k'} A_{jk}\frac{F_j}{t_j^2}A_{jk'}\Psi^v_{k'}, \tag{8a}$$

for scalar functions defined on cell centres ($\{\Psi^c\}_i \equiv \Psi^c_i$) and vertices ($\{\Psi^v\}_k \equiv \Psi^v_k$) respectively. On the dual network, these have analogues $\mathsf{L}_{\mathcal{C}} = -\widetilde{\mathrm{div}}^v\circ\mathrm{grad}^c = \widetilde{\mathrm{CURL}}^c\circ\mathrm{CURL}^c$ acting on cell centres and $\mathsf{L}_{\mathcal{T}} =$

$-\mathrm{div}^v \circ \widetilde{\mathrm{grad}}^v = \mathrm{CURL}^v \circ \widetilde{\mathrm{CURL}}^v$ on triangles, where

$$\{\mathsf{L}_{\mathcal{C}}\hat{\Psi}^c\}_i = A_i^{-1}\textstyle\sum_{j,i'} B_{ij}\dfrac{F_j}{T_j^2}B_{i'j}\hat{\Psi}^c_{i'}, \quad \{\mathsf{L}_{\mathcal{T}}\hat{\Psi}^v\}_k = E_k^{-1}\textstyle\sum_{j,k'} A_{jk}\dfrac{T_j^2}{F_j}A_{jk'}\hat{\Psi}^v_{k'}. \tag{8b}$$

(Throughout, hats distinguish functions defined on the dual network.). These definitions are summarised in (7). The four scalar Laplacians reduce to two ($\mathsf{L}_{\mathcal{T}} = \mathsf{L}_{\mathcal{V}}$, $\mathsf{L}_{\mathcal{F}} = \mathsf{L}_{\mathcal{C}}$) in the special case of edge-link orthogonality, when $F_j = T_j t_j$.

2.4 Helmholtz decomposition

A vector defined over edges or links can be represented in terms of potentials defined over each network, via a form of Helmholtz decomposition [21]. Assuming the cell monolayer is simply connected, any vector $\mathbf{h} \in \mathcal{E}$ with elements $\mathbf{h}_j$ ($j = 1, \dots, N_e$) has representation with regard to the primal network of the form [*explain proof*]

$$\mathbf{h} = \mathbf{h}^{\parallel} + \mathbf{h}^{\perp} \quad \text{where} \quad \mathbf{h}^{\parallel} = \mathrm{grad}^v\psi^v + \widetilde{\mathrm{curl}}^c\Psi^c \in \mathcal{E}^{\parallel} \quad \text{and} \quad \mathbf{h}^{\perp} = -\widetilde{\mathrm{grad}}^c\psi^c + \mathrm{curl}^v\Psi^v \in \mathcal{E}^{\perp}, \tag{9}$$

for some ψ^v and $\Psi^v \in \mathcal{V}$ (with components ψ^v_k, Ψ^v_k, $k = 1, \dots, N_v$), and for some ψ^c and $\Psi^c \in \mathcal{F}$ (with components ψ^c_i, Ψ^c_i, $i = 1, \dots, N_c$). Here $\mathbf{h}$ has been decomposed into its components parallel and perpendicular to each edge (note that $\mathrm{curl}^v = \boldsymbol{\epsilon}_k\mathrm{grad}^v$ and $-\widetilde{\mathrm{grad}}^c = \boldsymbol{\epsilon}_k\widetilde{\mathrm{curl}}^c$). It follows that

$$\mathrm{div}^c\,\mathbf{h} = \mathrm{div}^c\,\mathbf{h}^{\perp} = -\mathrm{div}^c \circ \widetilde{\mathrm{grad}}^c\psi^c = \mathsf{L}_{\mathcal{F}}\psi^c, \quad \mathrm{curl}^c\,\mathbf{h} = \mathrm{curl}^c\,\mathbf{h}^{\parallel} = \mathrm{curl}^c \circ \widetilde{\mathrm{curl}}^c\,\Psi^c = \mathsf{L}_{\mathcal{F}}\Psi^c, \tag{10}$$

and likewise $\mathsf{L}_{\mathcal{V}}\psi^v = -\widetilde{\mathrm{div}}^v\,\mathbf{h}$ and $\mathsf{L}_{\mathcal{V}}\Psi^v = \widetilde{\mathrm{curl}}^v\,\mathbf{h}$. The same vector can be represented over the dual network. Setting $\hat{\mathbf{h}} = \mathbf{h}$, the Helmholtz decomposition for a vector $\hat{\mathbf{h}} \in \mathcal{L}$ is given in terms of components parallel and perpendicular to links:

$$\hat{\mathbf{h}} = \hat{\mathbf{h}}^{\parallel} + \hat{\mathbf{h}}^{\perp} \quad \text{where} \quad \hat{\mathbf{h}}^{\parallel} = \mathrm{grad}^c\hat{\psi}^c + \widetilde{\mathrm{CURL}}^v\hat{\Psi}^v \in \mathcal{L}^{\parallel} \quad \text{and} \quad \hat{\mathbf{h}}^{\perp} = -\widetilde{\mathrm{grad}}^v\hat{\psi}^v + \mathrm{CURL}^c\hat{\Psi}^c \in \mathcal{L}^{\perp} \tag{11}$$

for some $\hat{\psi}^c, \hat{\Psi}^c \in \mathcal{C}$ and $\hat{\psi}^v, \hat{\Psi}^v \in \mathcal{T}$. Note that $\mathrm{CURL}^c = \boldsymbol{\epsilon}_i\mathrm{grad}^c$ and $-\widetilde{\mathrm{grad}}^v = \boldsymbol{\epsilon}_i\widetilde{\mathrm{CURL}}^v$. Then

$$\mathrm{div}^v\,\mathbf{h} = \mathrm{div}^v\,\hat{\mathbf{h}}^{\perp} = -\mathrm{div}^v \circ \widetilde{\mathrm{grad}}^v\hat{\psi}^v = \mathsf{L}_{\mathcal{T}}\hat{\psi}^v, \quad \mathrm{CURL}^v\,\mathbf{h} = \mathrm{CURL}^v\,\hat{\mathbf{h}}^{\perp} = \mathrm{CURL}^v\,\widetilde{\mathrm{CURL}}^v\,\hat{\Psi}^v = \mathsf{L}_{\mathcal{T}}\hat{\Psi}^v \tag{12a}$$

and likewise $\mathsf{L}_{\mathcal{C}}\psi^v = -\widetilde{\mathrm{div}}^c\,\hat{\mathbf{h}}$ and $\mathsf{L}_{\mathcal{C}}\Psi^v = \widetilde{\mathrm{CURL}}^c\,\hat{\mathbf{h}}$.

In summary, given a vector field $\mathbf{h}$, we can determine the 8 corresponding scalar potentials that provide representations relative to the primal and dual networks, by solving a sequence of Poisson problems using the four Laplacians given in (7).

[Clarify notation, particularly in use (or not) of i, j, k]

3 Discrete forces, stresses and potentials

3.1 Force potential and microstress

A standard computational implementation of the vertex model yields forces $\mathbf{f}_{ik}$ (of cell i, acting on vertex k) that balance at each vertex and around each cell, so that (respectively)

$$\textstyle\sum_i C_{ik}\mathbf{f}_{ik} = \mathbf{0}, \quad \sum_k C_{ik}\mathbf{f}_{ik} = \mathbf{0}. \tag{13}$$

These balances can be interpreted geometrically by rotating each force by $\pi/2$ (a form of Maxwell–Cremona force tiling [22]), so that forces form closed triangles around each vertex (13a) and closed loops around each cell (13b), as illustrated in Figure 3 below. The network of rotated forces is topologically equivalent to the network

of links connecting adjacent edge centroids [17]. Just as edge centroids provide a vector potential for these links, so the vertices of the network of rotated forces define a vector potential $\mathbf{h}_j$ for rotated forces, via

$$\mathbf{f}_{ik} = -\textstyle\sum_j \boldsymbol{\epsilon}_i B_{ij} \mathbf{h}_j A_{jk}, \tag{14}$$

such that $\mathbf{h}_j - \mathbf{h}_{j'} = \sum -\boldsymbol{\varepsilon}\mathbf{f}_{ik}$ [*check*], summing over a path connecting vertex j' to j [17]. The force stress $\boldsymbol{\sigma}_i^c$ of cell i (and the force stress $\boldsymbol{\sigma}_k^v$ defined over triangle k) can then be written as the first spatial moment of the forces acting on the cell (or triangle) [8], or equivalently in terms of the force potential $\mathbf{h}$ [17], as

$$A_i\boldsymbol{\sigma}_i^c = \textstyle\sum_k C_{ik}\mathbf{r}_k \otimes \mathbf{f}_{ik} = \sum_j B_{ij}(\mathbf{t}_j \otimes \mathbf{h}_j)\boldsymbol{\epsilon}_i, \quad E_k\boldsymbol{\sigma}_k^v = \textstyle\sum_j A_{jk}(\mathbf{T}_j \otimes \mathbf{h}_j)\boldsymbol{\epsilon}_k. \tag{15}$$

We see from (15) that $\boldsymbol{\sigma}^c \in \mathcal{E}^{\parallel} \times \mathcal{E}$ and $\boldsymbol{\sigma}^v \in \mathcal{L}^{\parallel} \times \mathcal{L}$.

The force-moment tensors in (15) are extensive and satisfy an important conservation principle [22]: summing $A_i\boldsymbol{\sigma}_i^c$ over adjacent cells yields a quantity defined entirely by forces or force potentials at the periphery of the cells (because of cancellation of internal forces for a system in equilibrium). In particular,

$$\textstyle\sum_i A_i\boldsymbol{\sigma}_i^c = -P_{\text{ext}}\mathsf{I}\mathcal{A} \tag{16}$$

for a monolayer of total area $\mathcal{A}$ that is subject to a uniform external pressure P_{ext} [8]. This property also makes it possible to consider how $A_i\boldsymbol{\sigma}_i^c$ or $E_k\boldsymbol{\sigma}_k^v$ are built from their component parts. Accordingly, we define the microscopic force stress as

$$A_i\tilde{\boldsymbol{\sigma}}_i^c = \cup_j B_{ij}(\mathbf{t}_j \otimes \mathbf{h}_j)\boldsymbol{\epsilon}_i, \quad E_k\tilde{\boldsymbol{\sigma}}_k^v = \cup_j A_{jk}(\mathbf{T}_j \otimes \mathbf{h}_j)\boldsymbol{\epsilon}_k. \tag{17}$$

Here B [A] attributes each edge [link] component to a neighbouring cell [triangle] face but maintains it as a distinct entity from the other edge [link] contributions. It follows immediately that $\mathbf{n}_{ij} \cdot \tilde{\boldsymbol{\sigma}}_i^c = 0$ for each edge j of cell i and $\mathbf{N}_{jk} \cdot \tilde{\boldsymbol{\sigma}}_k^v = 0$ for each link j of triangle k, ensuring that

$$\text{div}^c\, \tilde{\boldsymbol{\sigma}}_i^c = \mathbf{0} \quad \text{and} \quad \text{div}^v\, \tilde{\boldsymbol{\sigma}}_k^v = \mathbf{0}. \tag{18}$$

We decompose $\mathbf{h}_j$ into components along $\mathbf{t}_j$ and $\boldsymbol{\epsilon}_i\mathbf{t}_j$, so that

$$\begin{aligned} A_i\tilde{\boldsymbol{\sigma}}_i^c &= \cup_j B_{ij}\left[\hat{\mathbf{t}}_j \otimes \hat{\mathbf{t}}_j(\mathbf{h}_j \cdot \mathbf{t}_j) + \hat{\mathbf{t}}_j \otimes (\boldsymbol{\epsilon}_i\hat{\mathbf{t}}_j)(\mathbf{h}_j \cdot (\boldsymbol{\epsilon}_i\mathbf{t}_j))\right]\boldsymbol{\epsilon}_i \\ &= \cup_j B_{ij}\left[\hat{\mathbf{t}}_j \otimes \hat{\mathbf{n}}_{ij}(\mathbf{h}_j \cdot \mathbf{t}_j) + \hat{\mathbf{t}}_j \otimes \hat{\mathbf{t}}_j(\mathbf{h}_j \cdot (\boldsymbol{\epsilon}_i\mathbf{t}_j))\right]. \end{aligned} \tag{19}$$

Then $A_i\text{Tr}(\tilde{\boldsymbol{\sigma}}_i^c) = \sum_{j'} B_{ij'}\mathbf{h}_{j'} \cdot (\boldsymbol{\epsilon}_i\mathbf{t}_{j'})$ so that the deviatoric microscopic force stress becomes

$$A_i\tilde{\boldsymbol{\sigma}}_i^{cD} = \cup_j B_{ij}\left[\hat{\mathbf{t}}_j \otimes \hat{\mathbf{n}}_{ij}(\mathbf{h}_j \cdot \mathbf{t}_j) + \hat{\mathbf{t}}_j \otimes \hat{\mathbf{t}}_j(\mathbf{h}_j \cdot (\boldsymbol{\epsilon}_i\mathbf{t}_j))\right] - \tfrac{1}{2}\mathsf{I}\textstyle\sum_{j'} B_{ij'}\mathbf{h}_{j'} \cdot (\boldsymbol{\epsilon}_i\mathbf{t}_{j'}). \tag{20}$$

The final term involves $\sum_j$ rather than $\cup_j$, ensuring that $\text{div}^c\, \tilde{\boldsymbol{\sigma}}_i^{cD} = \mathbf{0}$. $\tilde{\boldsymbol{\sigma}}_i^{cD}$ has symmetric component

$$A_i\tilde{\boldsymbol{\sigma}}_i^{c(s)} = \cup_j B_{ij}\left[\tfrac{1}{2}(\hat{\mathbf{t}}_j \otimes \hat{\mathbf{n}}_{ij} + \hat{\mathbf{n}}_{ij} \otimes \hat{\mathbf{t}}_j)(\mathbf{h}_j \cdot \mathbf{t}_j) + \hat{\mathbf{t}}_j \otimes \hat{\mathbf{t}}_j(\mathbf{h}_j \cdot (\boldsymbol{\epsilon}_i\mathbf{t}_j))\right] - \tfrac{1}{2}\mathsf{I}\textstyle\sum_{j'} B_{ij'}\mathbf{h}_{j'} \cdot (\boldsymbol{\epsilon}_i\mathbf{t}_{j'}) \tag{21}$$

and antisymmetric component

$$A_i\tilde{\boldsymbol{\sigma}}_i^{c(a)} = \cup_j B_{ij}\tfrac{1}{2}(\hat{\mathbf{t}}_j \otimes \hat{\mathbf{n}}_{ij} - \hat{\mathbf{n}}_{ij} \otimes \hat{\mathbf{t}}_j)(\mathbf{h}_j \cdot \mathbf{t}_j) = \tfrac{1}{2}\boldsymbol{\epsilon}_i \cup_j B_{ij}(\mathbf{h}_j \cdot \mathbf{t}_j), \tag{22}$$

where we have used $\hat{\mathbf{t}}_j \otimes \hat{\mathbf{n}}_{ij} - \hat{\mathbf{n}}_{ij} \otimes \hat{\mathbf{t}}_j \equiv \boldsymbol{\epsilon}_i$ (consider its action on a vector $\alpha\hat{\mathbf{t}_j} + \beta\hat{\mathbf{n}}_{ij}$). We can therefore interpret $\mathbf{h}_j \cdot \mathbf{t}_j$ in (22) as a torque exerted on each edge of the cell. Analogous expressions to (19-22) follow immediately for $\tilde{\boldsymbol{\sigma}}_k$, after projecting $\mathbf{h}_j$ onto $\mathbf{T}_j$ and $\boldsymbol{\epsilon}_k\mathbf{T}_j$.

The cell and triangle force-stresses can be recovered from microstresses by replacing $\cup_j$ with $\sum_j$ in (17), as in [17], to give (15). It follows that

$$P_{\text{eff}i} \equiv \tfrac{1}{2}\text{Tr}(\boldsymbol{\sigma}_i^c) = -\tfrac{1}{2}\{\text{div}^c\, \mathbf{h}\}_i, \qquad \boldsymbol{\sigma}_i^{c(a)} = \tfrac{1}{2}\boldsymbol{\epsilon}_i\{\text{curl}^c\, \mathbf{h}\}_i, \tag{23a}$$

$$P_{\text{eff}k} \equiv \tfrac{1}{2}\text{Tr}(\boldsymbol{\sigma}_k^v) = -\tfrac{1}{2}\{\text{div}^v\, \mathbf{h}\}_k, \qquad \boldsymbol{\sigma}_k^{v(a)} = \tfrac{1}{2}\boldsymbol{\epsilon}_k\{\text{CURL}^v\, \mathbf{h}\}_k. \tag{23b}$$

With $\mathbf{t}_j \cdot \mathbf{T}_j \neq 0$ in general, we see how the projections of the vector force potential $\mathbf{h}$ onto edges and links (in curls) play a distinct role from the projections on normals to cells and triangles (in divergences).

3.2 Discrete stress potentials

We now pursue the discrete analogue of (1), expressing the force stress in terms of scalar potentials and identifying the associated couple stress vector. The force potential $\mathbf{h}$ can be expressed in terms of scalar potentials using (9) and (11), so that (23) becomes

$$\mathrm{Tr}(\boldsymbol{\sigma}_i^c) = -\{\mathsf{L}_{\mathcal{F}}\psi^c\}_i, \qquad \boldsymbol{\sigma}_i^{c(a)} = \tfrac{1}{2}\boldsymbol{\epsilon}_i\{\mathsf{L}_{\mathcal{F}}\Psi^c\}_i, \tag{24a}$$

$$\mathrm{Tr}(\boldsymbol{\sigma}_k^v) = -\{\mathsf{L}_{\mathcal{T}}\hat{\psi}^v\}_k, \qquad \boldsymbol{\sigma}_k^{v(a)} = \tfrac{1}{2}\boldsymbol{\epsilon}_k\{\mathsf{L}_{\mathcal{T}}\hat{\Psi}^v\}_k. \tag{24b}$$

We construct vectors orthogonal to $\mathbf{h}$, writing $\hat{\mathbf{h}} = \mathbf{h}$ as its representation over the dual triangulation, so that

$$-\boldsymbol{\epsilon}_i\mathbf{h} = (\mathrm{curl}^v\psi^v - \widetilde{\mathrm{grad}}^c\Psi^c) - (\widetilde{\mathrm{curl}}^c\psi^c + \mathrm{grad}^v\Psi^v), \tag{25a}$$

$$-\boldsymbol{\epsilon}_k\hat{\mathbf{h}} = (\mathrm{CURL}^c\hat{\psi}^c - \widetilde{\mathrm{grad}}^v\hat{\Psi}^v) - (\widetilde{\mathrm{CURL}}^v\hat{\psi}^v + \mathrm{grad}^c\hat{\Psi}^c). \tag{25b}$$

Then, by analogy with (48), we can re-write (15) as

$$\boldsymbol{\sigma}^c = \mathrm{curl}^c \otimes (-\boldsymbol{\epsilon}_i\mathbf{h}) \quad \text{and} \quad \boldsymbol{\sigma}^v = \mathrm{CURL}^v \otimes (-\boldsymbol{\epsilon}_k\hat{\mathbf{h}}). \tag{26}$$

We briefly verify the conditions in (24). Contracting expressions in (26) [*fix notation, check all terms*], $\mathrm{Tr}(\boldsymbol{\sigma}^c) = \mathrm{curl}^c \circ (-\boldsymbol{\epsilon}_i\mathbf{h}) = -\mathsf{L}_{\mathcal{F}}\psi^c$ (note that $\mathrm{curl}^c \otimes \mathrm{curl}^v = 0$ because of geometry and $\mathrm{curl}^c \otimes \mathrm{grad}^v = 0$ because of topology). Likewise $\mathrm{Tr}(\boldsymbol{\sigma}^v) = \mathrm{CURL}^v \circ (-\boldsymbol{\epsilon}_k\hat{\mathbf{h}}) = -\mathsf{L}_{\mathcal{T}}\hat{\psi}^v$. From (68),

$$(\mathrm{CURL}^v \otimes \widetilde{\mathrm{grad}}^v\hat{\Psi}^v)_{k,pq} = \frac{1}{E_k}\sum_{j,k'}\frac{\{\mathbf{T}_j \otimes (\boldsymbol{\epsilon}_k\mathbf{T}_j)\}_{pq}}{F_{j'}}A_{jk'}\hat{\Psi}^v_{k'}. \tag{27}$$

Using [CHECK]

$$\tfrac{1}{2}(\{\mathbf{T}_j \otimes (\boldsymbol{\epsilon}_k\mathbf{T}_j)\}_{pq} - \{\mathbf{T}_j \otimes (\boldsymbol{\epsilon}_k\mathbf{T}_j)\}_{qp}) = -\tfrac{1}{2}\boldsymbol{\epsilon}_k T_j^2 \tag{28}$$

we see that $(\mathrm{CURL}^v \otimes \widetilde{\mathrm{grad}}^v\hat{\Psi}^v)_k^{(a)} = -\frac{1}{2}\boldsymbol{\epsilon}_k\mathsf{L}_{\mathcal{T}}\hat{\Psi}^v$, and therefore (26) implies $\boldsymbol{\sigma}^{v(a)} = \frac{1}{2}\boldsymbol{\epsilon}_k\mathsf{L}_{\mathcal{T}}\hat{\Psi}^v$. Likewise $\boldsymbol{\sigma}^{c(a)} = \frac{1}{2}\boldsymbol{\epsilon}_i\mathsf{L}_{\mathcal{F}}\Psi^c$ [*Show that remaining antisymmetric components vanish.*]. In summary, (26) shows how the Cauchy stresses are defined in terms of the force potential $\mathbf{h}$, which is given in turn in terms of eight potentials (four per network) in (25). Explicitly,

$$\boldsymbol{\sigma}^c = \mathrm{curl}^c \otimes \left[(\mathrm{curl}^v\psi^v - \widetilde{\mathrm{grad}}^c\Psi^c)_\perp - (\widetilde{\mathrm{curl}}^c\psi^c + \mathrm{grad}^v\Psi^v)_\parallel\right], \tag{29a}$$

$$\boldsymbol{\sigma}^v = \mathrm{CURL}^v \otimes \left[(\mathrm{CURL}^c\hat{\psi}^c - \widetilde{\mathrm{grad}}^v\hat{\Psi}^v)_\perp - (\widetilde{\mathrm{CURL}}^v\hat{\psi}^v + \mathrm{grad}^c\hat{\Psi}^c)_\parallel\right], \tag{29b}$$

where subscripts $\perp$ and $\parallel$ serve as reminders of the orientations of the vectors relative to edges (for $\boldsymbol{\sigma}^c$) and links ($\boldsymbol{\sigma}^v$) respectively. We note also from (25) that

$$\mathbf{h} = \mathrm{grad}^v\psi^v - \widetilde{\mathrm{grad}}^c\psi^c - \boldsymbol{\mu}, \quad \boldsymbol{\mu} = -\widetilde{\mathrm{curl}}^c\Psi^c - \mathrm{curl}^v\Psi^v, \tag{30a}$$

$$\hat{\mathbf{h}} = \mathrm{grad}^c\hat{\psi}^c - \widetilde{\mathrm{grad}}^v\hat{\psi}^v - \hat{\boldsymbol{\mu}}, \quad \hat{\boldsymbol{\mu}} = -\widetilde{\mathrm{CURL}}^v\hat{\Psi}^v - \mathrm{CURL}^c\hat{\Psi}^c. \tag{30b}$$

suggesting how $(\Psi^v,\ \Psi^v)$ and $(\hat{\Psi}^v, \hat{\Psi}^c)$ can be interpreted as scalar potentials for the couple stress vector, in its representation over cells and over triangles. We note that $\mathrm{curl}^c\boldsymbol{\mu} = -\mathsf{L}_{\mathcal{F}}\Psi^c$ and $\mathrm{CURL}^v\hat{\boldsymbol{\mu}} = -\mathsf{L}_{\mathcal{T}}\hat{\Psi}^v$ so that

$$\boldsymbol{\sigma}^{c(a)} = -\tfrac{1}{2}\boldsymbol{\epsilon}_i\mathrm{curl}^c\boldsymbol{\mu}, \quad \boldsymbol{\sigma}^{v(a)} = -\tfrac{1}{2}\boldsymbol{\epsilon}_k\mathrm{curl}^c\boldsymbol{\mu}. \tag{31}$$

4 Introducing a constitutive model

4.1 Virtual work in the vertex model

We introduce an energy per cell $U_i = U(A_i, L_i)$ (assuming cells have homogeneous mechanical properties) and define a pressure and tension as $\mathcal{P}_i \equiv \partial U/\partial A_i$ and $\mathcal{T}_i \equiv \partial U/\partial L_i$ respectively. The total energy of the

monolayer is $\mathcal{U} = \sum_i U_i + P_{\text{ext}}\mathcal{A}$, where $\mathcal{A} = \sum_i A_i$ and P_{ext} is an external pressure applied to the periphery of the monolayer. We therefore assume there is no moment traction at the monolayer periphery and only a normal force traction. $\mathcal{U}$ is a function of vertex locations, via the dependence of areas and perimeters on $\mathbf{r}_k$. Suppose the monolayer is in a stationary equilibrium configuration (denoted with a prime) and consider virtual displacements $\delta\mathbf{r}_k$ of its vertices. The expansion

$$\mathcal{U} = \mathcal{U}' + \sum_{i,k} \left(\frac{\partial U_i}{\partial \mathbf{r}_k} + P_{\text{ext}} \frac{\partial A_i}{\partial \mathbf{r}_k} \right)' \cdot \delta\mathbf{r}_k + \sum_{i,k,k^\star} \delta\mathbf{r}_k \cdot \left(\frac{\partial^2 U_i}{\partial \mathbf{r}_k \partial \mathbf{r}_{k^\star}} + P_{\text{ext}} \frac{\partial^2 A_i}{\partial \mathbf{r}_k \partial \mathbf{r}_{k^\star}} \right)' \cdot \delta\mathbf{r}_{k^\star} + \dots \tag{32}$$

reveals the force $\partial U_i/\partial \mathbf{r}_k$ exerted at vertex k by cell i. Recall that $\partial A_i/\partial \mathbf{r}_k = -\frac{1}{2}\mathbf{n}_{ij}\overline{A}_{jk}$; it follows that $\sum_i \partial A_i/\partial \mathbf{r}_k$ vanishes at all internal tricellular junctions, so that P_{ext} contributes to forces only along the monolayer's periphery, via virtual displacement of edge centroids:

$$P_{\text{ext}} \textstyle\sum_{i,k} \left(\frac{\partial A_i}{\partial \mathbf{r}_k} \right)' \cdot \delta\mathbf{r}_k = -\frac{1}{2} P_{\text{ext}} \sum_{i,j,k} \overline{A}_{jk} \mathbf{n}'_{ij} \cdot \delta\mathbf{r}_k = -P_{\text{ext}} \sum_{i,j} \mathbf{n}'_{ij} \cdot \delta\mathbf{c}_j. \tag{33}$$

The sum of all forces at each vertex vanishes when the monolayer is at an equilibrium, i.e. $\sum_i C_{ik}(\partial U_i/\partial \mathbf{r}_k + P_{\text{ext}}\partial A_i/\partial \mathbf{r}_k)' = \mathbf{0}$ for all k, as in (13). The second variation in (32) captures weakly nonlinear effects and establishes the stability or otherwise of the equilibrium [23]. We work below with the first variation, but consider how the forces organise into stresses acting over cells.

It is sufficient for our purposes to restrict attention to variations that can be expressed as a smooth function of position under a deformation $\mathbf{u}(\mathbf{x})$, i.e. we map vertices from $\mathbf{r}'_k$ to $\mathbf{r}_k = \mathbf{r}'_k + \mathbf{u}(\mathbf{r}'_k)$ so that $\delta\mathbf{r}_k = \mathbf{u}(\mathbf{r}'_k)$. In the following, we will neglect effects that are quadratic in $\mathbf{u}$ but account for first- and second-order deformation gradients $\nabla\mathbf{u}$ and $\mathsf{M} \equiv (\nabla \otimes \nabla)\mathbf{u}$. We will then reformulate the first variation in (32) in terms of $\mathsf{E} \equiv \frac{1}{2}(\nabla\mathbf{u} + \nabla\mathbf{u}^\top)$, $\nabla\mathsf{E}$ and $\boldsymbol{\kappa} \equiv -\frac{1}{4}(\nabla^2\mathbf{u} - \nabla(\nabla\cdot\mathbf{u}))$, to determine the conjugate stresses. We will gather terms over cells, and also repartition them over the dual triangulation, to identify stresses over cells and triangles. In doing so, we interpolate deformation gradients evaluated on vertices onto edge centroids and cell centres, using Taylor expansion to capture the leading-order effect of spatial variations. Accordingly, we use subscripts i, j and k to describe fields evaluated at cell centres, edge centroids and vertices, writing $\mathbf{u}_i \equiv \mathbf{u}(\mathbf{R}'_i)$, $\mathbf{u}_j \equiv \mathbf{u}(\mathbf{c}'_j)$ and $\mathbf{u}_k = \mathbf{u}(\mathbf{r}'_k)$ and so on.

We retain second derivatives of $\mathbf{u}$ but discard third and higher derivatives, assuming deformations vary over scales long compared to the size of individual cells. As shown in Appendix C, the changes in cell perimeter and area to this order are

$$L_i = L'_i \left[1 + \mathsf{Q}_i : \mathsf{E}_i + \mathsf{X}_i \vdots (\nabla\mathsf{E})_i \right], \tag{34a}$$

$$A_i = A'_i \left[1 + \mathsf{I} : \mathsf{E}_i + \mathsf{Y}_i \vdots (\nabla\mathsf{E})_i + \left[\frac{1}{8A'_i} \textstyle\sum_j (t'_j)^2 \mathbf{n}'_{ij} \right] \cdot \boldsymbol{\kappa}_i \right], \tag{34b}$$

where $L'_i\mathsf{Q}_i \equiv \sum_j \overline{B}_{ij}\mathbf{t}'_j \otimes \hat{\mathbf{t}}'_j$. The third-order tensors X_i and Y_i (see (83, 88)) characterise the impact of strain gradients on cell perimeter and area respectively. They are size-dependent, as is appropriate for objects that measure a gradient. The antisymmetric component of E does not change perimeter to this order, but its gradient alters cell area through the curvature $\boldsymbol{\kappa}$.

Returning to (32), the energy maps from $\mathcal{U}_0 \equiv \mathcal{U}' + P_{\text{ext}}\mathcal{A}'$ to

$$\begin{aligned}
\mathcal{U} + P_{\text{ext}}\mathcal{A} &= \textstyle\sum_i [U_i(A_i, L_i) + P_{\text{ext}} A_i] \\
&= \mathcal{U}_0 + \textstyle\sum_i [\mathcal{P}'_i(A_i - A'_i) + \mathcal{T}'_i(L_i - L'_i)] - P_{\text{ext}} \sum_{i,j} \mathbf{n}_{ij} \cdot (\mathbf{c}_j - \mathbf{c}'_j) + \dots \\
&= \mathcal{U}_0 + \textstyle\sum_i \left\{ A'_i \boldsymbol{\sigma}_i^{(s)} : \mathsf{E}_i + (\mathcal{P}_i A'_i \mathsf{Y}_i + \mathcal{T}_i L'_i \mathsf{X}_i) \vdots \nabla\mathsf{E}_i - 2A'_i \boldsymbol{\mu}_i^c \cdot \boldsymbol{\kappa}_i \right\} - P_{\text{ext}} \textstyle\sum_{i,j} \mathbf{n}'_{ij} \cdot \mathbf{u}_j + \dots,
\end{aligned} \tag{35}$$

using (34) and neglecting quantities that are quadratic in strains. We also use (80) to show that $\mathbf{n}_{ij} \cdot (\mathbf{c}_j - \mathbf{c}'_j) = \mathbf{n}_{ij} \cdot \mathbf{u}_j$ to this order, so that P_{ext} does not exert any moment on the periphery. Applying the principle of virtual

work by setting the first variation in (35) to zero, comparison with (50) reveals the leading-order symmetric force-stress tensor and couple stress vector of cell i as

$$\boldsymbol{\sigma}_i^{c(s)} = \mathcal{P}_i' \mathbf{I} + \frac{\mathcal{T}_i' L_i'}{A_i'} \mathsf{Q}_i, \quad \boldsymbol{\mu}_i^c = -\frac{\mathcal{P}_i'}{16 A_i'} \textstyle\sum_j (t_j')^2 \mathbf{n}_{ij}'. \tag{36}$$

The isotropic stress has magnitude $P_{\text{eff},i}^c = \mathcal{P}_i' + \frac{1}{2}\mathcal{T}_i' L_i'/A_i'$. Given that $\sum_j \mathbf{n}_{ij}' = \mathbf{0}$, the couple stress vector vanishes for symmetric cells, for which t_j' is uniform. For now, we distinguish $\boldsymbol{\sigma}$ and $\boldsymbol{\mu}$ (the stresses derived from virtual work) from $\boldsymbol{\sigma}$ and $\boldsymbol{\mu}$ (the stresses derived from computed force potentials).

It is important to draw a distinction between $\boldsymbol{\sigma}_i^{c(s)}$ in (36), the force stress integrated over cell i, and the corresponding *microscopic* cell stress

$$\tilde{\boldsymbol{\sigma}}_i^{c(s)} = \mathcal{P}_i' \mathbf{I} + \frac{\mathcal{T}_i'}{A_i'} \cup_j \overline{B}_{ij} \mathbf{t}_j' \otimes \hat{\mathbf{t}}_j', \tag{37}$$

which retains edge-to-edge variation rather than averaging over the perimenter. This stress has zero divergence, because evaluating $\text{div}^c \tilde{\boldsymbol{\sigma}}_i^{c(s)}$ using (71) includes $\sum_j \mathbf{n}_{ij}'$ summed around a closed loop, which vanishes, and $\sum_j \mathbf{n}_{ij}' \cdot \mathbf{t}_j' \otimes \hat{\mathbf{t}}_j'$, which also vanishes as $\mathbf{n}_{ij}' \cdot \mathbf{t}_j' = 0$ along each edge. This ensures zero net force on each cell as in (13).

Repartitioning the first variation of energy over kites allows the stress over tristars to be expressed explicilty, as shown in Appendix D. It is also helpful to repartition the contribution to the energy associated with the couple stress vector. As gradients in curvature across the monolayer will not play a role in what follows, we take $\boldsymbol{\kappa}$ to be uniform, and drop primes, to define the couple-stress vector attributed to edges as

$$\textstyle\sum_i A_i(-2\boldsymbol{\mu}_i^c \cdot \boldsymbol{\kappa}) = \sum_j \frac{1}{2} F_j (-2\boldsymbol{\mu}_j \cdot \boldsymbol{\kappa}) \quad \text{where} \quad \boldsymbol{\mu}_j = -\frac{t_j^2}{8F_j} \textstyle\sum_i \mathcal{P}_i \mathbf{n}_{ij}, \tag{38}$$

where area is partitioned into trapezia of area $\frac{1}{2}F_j$, associated with edge/link j. $\boldsymbol{\mu}$ has zero curl around cells (because it acts along normals to edges and sits in the vector space $\mathcal{E}^\perp$), but has non-zero curl around triangles of the dual network:

$$\mathcal{C}_k \equiv \{\text{CURL}^v \boldsymbol{\mu}\}_k = E_k^{-1} \textstyle\sum_j A_{jk} \mathbf{T}_j \cdot \boldsymbol{\mu}_j = \frac{1}{8E_k} \sum_{i,j} \mathcal{P}_i B_{ij} t_j^2 A_{jk}. \tag{39}$$

As shown in (31), this can be related to the torque experienced in the neighbourhood of tricellular junction k. The pressure difference across edge j, $\sum_i B_{ij}\mathcal{P}_i$, is multiplied by t_j^2 to give a moment, and the three contributions to the moment at the tricellular junction are summed at the vertex. $\mathcal{C}_k$ vanishes if pressures are uniform ($\sum_i \mathcal{P}_i B_{ij} = 0$) or if the edges are of uniform size (because $\mathsf{BA} = \mathsf{0}$). We do not seek to impose any conditions on $\text{div}^c \boldsymbol{\mu}$ or $\text{div}^v \boldsymbol{\mu}$.

The couple traction on a surface of the cell with normal $\mathbf{n}$ is $m = \mathbf{n} \cdot \boldsymbol{\varepsilon} \boldsymbol{\mu}$. Thus the net couple traction on a cell vanishes because $\boldsymbol{\mu}_j$ on each edge is parallel to $\mathbf{n}_{ij}$ in (38).

4.2 Potentials for the vertex model

We now return to the representation of force potential using scalar potentials (9) and (11). To ensure zero couple on cells, we take $\Psi^c = 0$. Then $\text{curl}^c \mathbf{h}$ vanishes (so that $\boldsymbol{\sigma}_i^{(a)} = \mathsf{0}$ in (23)) but $\text{CURL}^v \mathbf{h} = \mathsf{L}_{\mathcal{T}} \hat{\Psi}^v$ is non-zero (giving non-zero torque on triangles). We identify (from (30a)) the couple stress vector $\boldsymbol{\mu}$ with $-\text{curl}^v \Psi^v$, which is normal to edges, satisfying $\text{div}^c \boldsymbol{\mu} = \mathbf{0}$. In general we expect $\boldsymbol{\mu}$ to be described by non-zero $\hat{\Psi}^v$ and $\hat{\Psi}^c$ in (30b).

A strategy for determining potentials is as follows. First, note from (77) the requirement to account for forcing

integrated across the monolayer. In particular, using (23) and (16),

$$[\mathbb{1}, \mathrm{div}^c\, \mathbf{h}]_{\mathcal{F}} = -\,2[\mathbb{1}, P_{\mathrm{eff}i}] = -2\textstyle\sum_i A_i P_{\mathrm{eff}i} = -2\mathcal{A}P_{\mathrm{ext}} \tag{40a}$$

$$[\mathbb{1}, \mathrm{div}^v\, \mathbf{h}]_{\mathcal{V}} = -\,2[\mathbb{1}, P_{\mathrm{eff}i}] = -2\textstyle\sum_i E_k P_{\mathrm{eff}k} \tag{40b}$$

$$[\mathbb{1}, \mathrm{curl}^c\, \mathbf{h}]_{\mathcal{F}} = 0 \tag{40c}$$

$$[\mathbb{1}, \mathrm{CURL}^v\, \mathbf{h}]_{\mathcal{V}} = -\,[\mathbb{1}, \mathrm{CURL}^v\, \boldsymbol{\mu}]_{\mathcal{V}} = -\tfrac{1}{8}\textstyle\sum_{i,j,k} \mathcal{P}_i B_{ij} t_j^2 A_{jk} \tag{40d}$$

(explain global constraint on stress - should the global torque vanish?). For each global effect, there will be a contribution to the potential, supplemented with local contributions.

1. On the primal network, solve $\mathsf{L}_{\mathcal{F}}\psi^c = \mathrm{div}^c\, \mathbf{h}$ (subject to suitable boundary conditions) to determine ψ^c.
2. With $\Psi^c = 0$, determine ψ^v as a line integral of $\mathbf{h}^{\parallel}$ (or use $\mathsf{L}_{\mathcal{V}}\psi^v = -\widetilde{\mathrm{div}}^v \mathbf{h}$).
3. With $\mathrm{div}^c\, \boldsymbol{\mu} = 0$, determine Ψ^v as a line integral of $\boldsymbol{\mu}$ (or use $\mathsf{L}_{\mathcal{V}}\Psi^v = \widetilde{\mathrm{curl}}^v \mathbf{h}$).
4. On the dual network, solve $\mathsf{L}_{\mathcal{T}}\hat{\psi}^v = \mathrm{div}^v \mathbf{h}$ (subject to suitable boundary conditions) to determine $\hat{\psi}^v$.
5. Solve $\mathsf{L}_{\mathcal{T}}\hat{\Psi}^v = \mathrm{CURL}^v \mathbf{h}$ to determine $\hat{\Psi}^v$.
6. Use $\mathsf{L}_{\mathcal{C}}\hat{\psi}^c = -\widetilde{\mathrm{div}}^c \mathbf{h}$ to determine $\hat{\psi}^c$.
7. Use $\mathsf{L}_{\mathcal{C}}\hat{\Psi}^c = \widetilde{\mathrm{CURL}}^c \mathbf{h}$ to determine $\hat{\Psi}^c$.

The potentials on the dual network depend on the choice of cell centres, because the forcing terms in steps 4 to 7 depend on the definition of links. However that when edges and links are orthogonal, $\mathsf{L}_{\mathcal{C}} = \mathsf{L}_{\mathcal{F}}$ and $\mathrm{div}^c = -\widetilde{\mathrm{div}}^c$, so that steps 1 and 6 are identical and $\hat{\psi}^c = \psi^c$; $\mathsf{L}_{\mathcal{V}} = \mathsf{L}_{\mathcal{T}}$ and $\mathrm{div}^v = -\widetilde{\mathrm{div}}^v$ so that steps 2 and 4 are identical and $\hat{\psi}^v = \psi^v$; $\mathrm{CURL}^v = \widetilde{\mathrm{curl}}^v$ so that steps 3 and 5 are identical and $\hat{\Psi}^v = \Psi^v$; and $\widetilde{\mathrm{CURL}}^c = \mathrm{curl}^c$ so that $\hat{\Psi}^c = 0$ in step 7. (Where a potential is uniformly constant, we take it to be zero without loss of generality.)

Each Laplacian can be expected to have a zero eigenvalue ($\lambda_1 = 0$) and a corresponding eigenvector $\mathbf{e}_1 = \mathbb{1} = (1, 1, \ldots, 1)^\top$. The remaining eigenvalues and eigenvectors can be used to construct the inverse, recognising the gauge invariance of each potential. For solubility, we expect to use the constraint $\mathbb{1}^\top \psi = 0$ in each case.

[*Uniqueness and solubility of the Laplacian problems needs to be established.*]

The present formulation leads to Airy stress functions ψ_i^c and ψ_k^v defined on centres and vertices. Previously the Airy stress function ψ_{ik} was allocated to kites. It is possible to relate the two representations. However the advantage of distributing the Airy function over centres and vertices is that its derivation in terms of positive semi-definite Laplacians is much more secure.

Relate potentials defined over kites to scalars ψ^c, ψ^v:

$$\mathbf{h}_j = \{\mathrm{CURL}^c\, \boldsymbol{\Psi}^c\}_j + \{\mathrm{curl}^v\, \boldsymbol{\Psi}^v\}_j + \{\mathrm{grad}^c\, \boldsymbol{\psi}^c\}_j + \{\mathrm{grad}^v\, \boldsymbol{\psi}^v\}_j \tag{41}$$

$$\equiv \frac{\boldsymbol{\epsilon}_k \mathbf{T}_j}{T_j^2}\textstyle\sum_i B_{ij}\Psi_i + \frac{\boldsymbol{\epsilon}_i \mathbf{t}_j}{t_j^2}\sum_k A_{jk}\Psi_k + \frac{\mathbf{T}_j}{T_j^2}\sum_i \overline{A}_{jk} B_{ij}\psi_{ik} + \frac{\mathbf{t}_j}{t_j^2}\sum_k A_{jk}\overline{B}_{ij}\psi_{ik} \tag{42}$$

[*Take couple stress and perturb to find resistance to bending. For an isotropic material, $\boldsymbol{\mu} = -8\eta\boldsymbol{\kappa}$ [20], where η is the couple stress coefficient, complementing traditional elastic moduli (or Lamé constants).*]

5 Computations

We implemented the vertex model using the cell energy

$$U(A_i, L_i) = \tfrac{1}{2}(A - A_i)^2 + \tfrac{1}{2}\Gamma(L_i - L_0)^2 \tag{43}$$

Figure 3: Simulation showing (a) a monolayer at equilibrium, (b) the associated rotated force network. Parameter values are $\Gamma =?$, $L_0 =?$, $P_{\text{ext}} =?$ (a) shows cells defined by vertices and edges, and the dual network defined by the triangulation connecting adjacent cell centroids. For peripheral cells, links connect cell centroids to edge centroids following (2). The vertices of the force network are force potentials $\mathbf{h}_j$.

Figure 4: For the equilibrium state shown in Figure 3(a), we show (a) $-\frac{1}{2}\{\text{div}^c\,\mathbf{h}\}_i$, giving the effective pressure in cells, (b) $-\frac{1}{2}\{\text{div}^v\,\mathbf{h}\}_k$, giving the effective pressure over triangles and (c) $\{\text{CURL}^v\,\mathbf{h}\}_k$ giving a measure of the couple in the neighbourhood of each vertex.

for which cell pressure and tension are linear in area and perimeter: $\mathcal{P}_i = A_i - 1$ and $\mathcal{T}_i = \Gamma(L_i - L_0)$. A vertex drag model was implemented so that $\eta \mathrm{d}\mathbf{r}_k/\mathrm{d}t = \sum_i C_{ik}\mathbf{f}_{ik}$ for some $\eta > 0$. We chose Γ and L_0 to take values for which the monolayer in a jammed state. An isolated monolayer under uniform external pressure P_{ext} was established by starting with a small number of cells and allowing cell divisions to occur randomly for an interval, prior to a period in which the monolayer settles to an equilibrium state.

The forces $\mathbf{f}_{ik}$ acting at each vertex in the equilibrium state were rotated and assembled to form a force network, as illustrated in Figure 3. The three rotated forces around each internal vertex form a closed triangle, and the Z_i forces around cell i form closed loops, confirming (13). For sufficiently large $|P_{\text{ext}}|$, the force network forms a planar graph (because the vertex force stress tensor maps the triangle connecting adjacent edge centroids around a vertex to the corresponding triangle of forces; the ratio of areas is given by $\det(\boldsymbol{\sigma}^v)$ [17]; large $|P_{\text{ext}}|$ increases the area of the force triangle). However in general this is not the case, although the force network maintains the same topology as that of connections between adjacent edge centroids [17]. The distorted force loops provide a striking illustration of the loading experienced by individual cells, and the heterogeneity between cells.

The vertices $\mathbf{h}_j$ of the rotated force network were then used to evaluate predictions of the model. We evaluated $-\frac{1}{2}\{\text{div}^c\,\mathbf{h}\}_i$ and confirmed that it recovered $P_{\text{eff}i}$ (Figure 4a), while $\text{div}^v\,\mathbf{h}$ gives the corresponding effective pressure partitioned over triangles (Figure 4b). We validated the prediction that $\text{curl}^c\,\mathbf{h} = 0$, but found that $\text{CURL}^v\,\mathbf{h}$ typically has a heterogeneous distribution over triangles (Figure 4d). [*Test against (39)*, using $\text{CURL}^v\mathbf{h} = -\text{CURL}^v\boldsymbol{\mu}$.]

We evaluated the Laplacians $\mathsf{L}_\mathcal{V}$, $\mathsf{L}_\mathcal{F}$, $\mathsf{L}_\mathcal{T}$, $\mathsf{L}_\mathcal{C}$ (8), checking that each is positive semi-definite. $\mathsf{L}_\mathcal{V}$ has identical structure to $\mathsf{L}_\mathcal{T}$ (likewise $\mathsf{L}_\mathcal{C}$ and $\mathsf{L}_\mathcal{F}$) and since links and edges are almost (but not exactly) orthogonal, the spectra and modes qualitatively similar. The first 16 modes of $\mathsf{L}_\mathcal{T}$ and $\mathsf{L}_\mathcal{C}$ are show in Figure 5.

Check that the eigenmodes of $\mathsf{L}_\mathcal{V}$ *and* $\mathsf{L}_\mathcal{T}$ *are orthogonal under the inner product* $[\cdot,\cdot]_\mathcal{V}$ *and that the eigenmodes of* $\mathsf{L}_\mathcal{F}$ *and* $\mathsf{L}_\mathcal{C}$ *are orthogonal under the inner product* $[\cdot,\cdot]_\mathcal{F}$.

Solve for the seven potentials via Sec. 4.2.

Force networks: used in granular flows [24] and suspensions [25].

Force chains: within cell monolayers or associated with cells embedded in matrix [26], mechanism for long-range signalling, inherently discrete structures

Confluence assumed [27], no fluctuations, no motility, slippage of adjacent junctions [28]

6 Discussion

Continuum mechanical models are widely used to describe biological tissues, and do so successfully over length-scales that are large in comparison to a tissue's internal heterogeneities. However at scales comparable to individual cells, the inherent granularity of the tissue becomes evident and the continuum hypothesis is violated. The vertex model [29, 1, 2, 4, 5] is one of a class of discrete models of tissue mechanics that resolves stresses at the level of individual cells, exploiting the natural partitioning of space that they provide. This offers

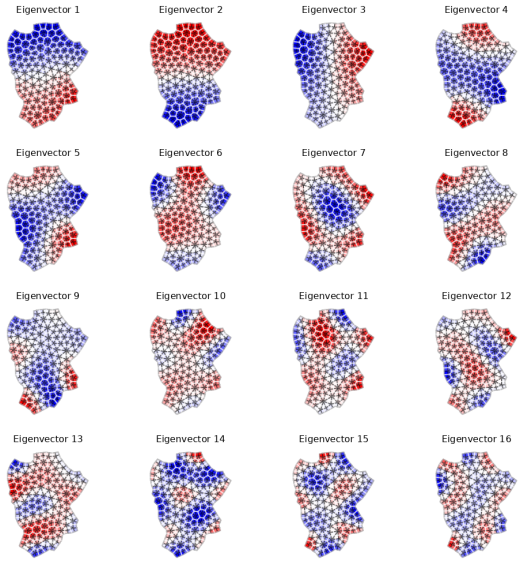

Figure 5: [Placeholder] Eigenmodes of $\mathsf{L}_{\mathcal{T}}$ for the equilibrium state shown in Figure 3. Mode 1 is uniform and should be presented as such.

immediate advantages in modelling growth processes, by allowing cell division, expansion and rearrangement to be represented explicitly. Likewise, explicit representation of individiual cells facilitates the description of subcellular processes (such as the cell cycle, or cell signalling) and enables direct comparison with images. Continuum models rely on assumed strain energy functions, expressed in terms of strain invariants; in contrast, the vertex model relies on a mechanical energy defined in terms of easily measured geometric invariants (such as the area or perimeter of cells in a planar monolayer). Despite these differences in the approach to constitutive modelling, a Cauchy stress can be defined in both instances.

In continua, it is commonly assumed that the Cauchy stress is symmetric, reflecting the absence of net torque on the smallest material elements; accordingly, stresses on material elements are fully determined by local strains. In a discrete model, however, the smallest elements (individual cells, or the triangles between adjacent cell centres) have finite size: stresses are specified primarily by local geometric measures (changes in cell area and perimeter induced by strains) but also by spatial gradients of strain, 'measured' across the length of an individual element. Deformations that generate appropriate bending deformations may thereby generate torques on tissue elements that are accommodated by so-called couple stresses. The present study is the first (to our knowledge) to address this feature in models of multicellular tissues, by defining the couple stress associated with the traditional vertex model. Our study of passive torques in epithelia is distinct from that of Yamamoto et al. [30], who consider active cortical torque generation in a vertex model using a 'disk-shaft' mechanism.

The strain energy that we chose to investigate here () passes a number of basic tests. Imposing forces at cell vertices is sufficient to ensure zero net force on each cell. This is demonstrated by closed loops in the plane of rotated forces (Figure X). The model also ensures zero net torque on individual cells, and a stress tensor that is symmetric (which we validated numerically). The stress of a cell can be constructed by summing contributions from individual vertices (or equivalently, from individual edges). These contributions can be repartitioned to evaluate the stress over the triangulation connecting cell centres. Here, in contrast, we find that the stress is asymmetric (Figure X), implying that a torque is exerted in the neighbourhood of each tricellular junction. This arises from pressure differences between the three cells neighbouring the junction, acting over edges of different lengths, creating a net moment. A couple stress must be incorporated in order to accommodate the torque.

An array of confluent polygonal cells provides a natural unstructured mesh on which to perform computations. The machinery for pursuing such calculations is provided by discrete exterior calculus (developed using tools of algebraic topology [31, 18] and mimetic finite differences (developed for numerical analysis [21, 32]). Incidence

matrices A and B encode topological relationships between cell vertices, edges and faces, and the equivalent relationships over the dual triangulation. When combined with appropriate metric information, they can be used to construct discrete differential operators. By respecting the need to preserve exact sequences, a full set of operators can be identified, including positive-semi-definite discrete Laplacians defined over the primal (cell) and dual (triangular) networks (Figure 2). Because links between cell centres are not typically orthogonal to cell edges, eight primary and eight derived operators must be considered. These enable Helmholtz–Hodge decomposition to be undertaken (for a monolayer with no holes), enabling a vector field defined over cell edges (namely, a force potential built from the forces acting on cell vertices) to be represented in terms of scalar potentials on each network. Thereby, we recover the discrete analogues of the Airy stress function of traditional 2D continuum elasticity, and the additional function introduced by Mindlin to describe couple stresses. In general, the functions derived over networks of cells are distinct from those derived over the dual triangulation.

With this framework in place, we return to a question raised previously [17], namely the consequence of neglecting torque balance in computational implementation of the vertex model. If couple stresses are assumed not to exist, so that all stresses are symmetric (over cells and over the dual triangulation), then cell edges and links between cell centres must be orthogonal. Indeed, a stronger condition was identified (that vertices sit at the orthocentre of the triangle formed by their neighbours [17]), which suppresses shearing deformations and is typically violated in real monolayers. Invoking couple stress relaxes the orthogonality (and orthocentricity) constraint. *Simple geometric measures of torque?*

The present analysis of force-stress and couple-stress in cellular monolayers is linear but weakly nonlocal. We used the principle of virtual work to define stresses, as variables conjugate to strains and strain gradients, but we did not consider second variations of the energy or perturbations of stresses to define elastic moduli [9]. Similarly, we have considered only systems at equilibrium, and not have not accounted for transient viscous effects. However this assessment of the vertex model demonstrates its utility in crossing scales from cell to tissue. Identifying the Laplacians of the cellular network opens the door for spectral methods to capture global modes of deformation of a tissue in a systematic way. Further, by demonstrating the necessity of accounting for couple stresses if torques are to be properly accounted for at the level of individual cells, we raise the question of the possible biological consequences of such couples in the neighbourhood of tricellular junctions, and the potential requirement to model tissues at the macroscopic level as couple-stress materials.

The curl of a scalar field (the Mindlin stress function) defined on vertices defines a couple stress vector defined on links; a further curl defines the torque on vertices as a vertex Laplacian of the stress function.

Explain microstress versus averaged stress.

Discuss alternative definitions of cell centres.

(Apart from neglecting couple stresses, the terms $(\hat{\mathbf{t}}_j \otimes \hat{\mathbf{t}}_j - \frac{1}{2}\mathsf{I})$ and $(\hat{\mathbf{T}}_j \otimes \hat{\mathbf{T}}_j - \frac{1}{2}\mathsf{I})$ in (**??**) were erroneously omitted in (3.33, 3.34) of [17].)

[*In introducing couple stresses, we must relax the stress-geometry condition identified in [17] involving the fabric tensor that measures the asymmetry of each tristar.*]

[*Show that orthocentricity implies zero couple stress.*]

Dynamics. Minimise Lagrangian $\mathcal{L}(\dot{\mathbf{r}}) = \Phi + \zeta(\dot{U} + \Phi)$ where $\Phi = \Phi(\dot{A}, \dot{L})$ is rate of dissipation.

Acknowledgements

BBSRC sLoLa. Leverhulme.

A Couple stress in continua

In two dimensions, a continuous simply-connected couple-stress material in plane strain can be characterised by a force-stress tensor $\boldsymbol{\sigma}$ (having zero divergence, ensuring force balance) and couple-stress vector $\boldsymbol{\mu}$, with the antisymmetric component of $\boldsymbol{\sigma}$ expressed as a curl of $\boldsymbol{\mu}$ (ensuring torque balance). There are three independent components of the symmetric component of force stress $\boldsymbol{\sigma}^{(s)} \equiv \frac{1}{2}(\boldsymbol{\sigma} + \boldsymbol{\sigma}^\top)$ and two of $\boldsymbol{\mu}$, constrained by two (scalar) force balances and a torque balance. These constraints are satisfied by expressing $\boldsymbol{\sigma}$ and $\boldsymbol{\mu}$ in terms of two potentials, the Airy stress function $\psi(\mathbf{x})$ plus a second stress function $\Psi(\mathbf{x})$ described by Mindlin [19], such that [20]

$$\sigma_{pq} = \varepsilon_{pr}\partial_r(\varepsilon_{qs}\partial_s\psi - \partial_q\Psi), \quad \mu_p = -\varepsilon_{pq}\partial_q\Psi, \tag{44}$$

ensuring that $\partial_p\sigma_{pq} = 0$ ($\operatorname{div}\boldsymbol{\sigma} = \mathbf{0}$) and $\partial_p\mu_p = 0$ ($\operatorname{div}\boldsymbol{\mu} = 0$). Here $\boldsymbol{\varepsilon}$ is the 2D Levi-Civita tensor representing a clockwise $\pi/2$ rotation. Equivalently, in Cartesians,

$$\sigma_{xx} = \partial_y^2\psi - \partial_x\partial_y\Psi, \quad \sigma_{yy} = \partial_x^2\psi + \partial_x\partial_y\Psi, \quad \sigma_{xy} = -\partial_x\partial_y\psi - \partial_y^2\Psi, \quad \sigma_{yx} = -\partial_x\partial_y\psi + \partial_x^2\Psi \tag{45}$$

with $\mu_y = \partial_x\Psi$ and $-\mu_x = \partial_y\Psi$. This formulation makes minimal constitutive assumptions beyond material continuity, except that the condition $\operatorname{div}\boldsymbol{\mu} = 0$ is a compatibility condition for an isotropic linearly elastic material rather than an equilibrium condition [20]. The Airy stress function ψ determines the isotropic component of the force-stress via $\operatorname{Tr}(\boldsymbol{\sigma}) = \nabla^2\psi$, while the Mindlin stress function Ψ determines the antisymmetric force stress via the torque balance $\boldsymbol{\sigma}^{(a)} \equiv \frac{1}{2}(\boldsymbol{\sigma} - \boldsymbol{\sigma}^\top) = -\frac{1}{2}\boldsymbol{\varepsilon}\nabla^2\Psi = -\frac{1}{2}\boldsymbol{\varepsilon}(\partial_x\mu_y - \partial_y\mu_x)$. The force stress can be decomposed into isotropic, antisymmetric and symmetric-deviatoric parts as

$$\boldsymbol{\sigma} = \tfrac{1}{2}\mathsf{I}\nabla^2\psi - \tfrac{1}{2}\boldsymbol{\varepsilon}\nabla^2\Psi + \boldsymbol{\sigma}^{(s)}, \quad \boldsymbol{\sigma}^{(s)} \equiv \begin{pmatrix} \frac{1}{2}(\partial_y^2 - \partial_x^2)\psi - \partial_x\partial_y\Psi & -\partial_x\partial_y\psi - \frac{1}{2}(\partial_y^2 - \partial_x^2)\Psi \\ -\partial_x\partial_y\psi - \frac{1}{2}(\partial_y^2 - \partial_x^2)\Psi & \frac{1}{2}(\partial_x^2 - \partial_y^2)\psi + \partial_x\partial_y\Psi \end{pmatrix}, \tag{46}$$

where $\operatorname{Tr}(\boldsymbol{\sigma}^{(s)}) = 0$. $\boldsymbol{\sigma}^{(s)}$ has real eigenvalues $\pm\lambda$, with $\lambda \geq 0$ measuring shear, which depends on both ψ and Ψ via

$$\lambda = \sqrt{\left[\tfrac{1}{2}(\partial_y^2 - \partial_x^2)\psi - \partial_x\partial_y\Psi\right]^2 + \left[\partial_x\partial_y\psi + \tfrac{1}{2}(\partial_y^2 - \partial_x^2)\Psi\right]^2}. \tag{47}$$

Writing $\mathbf{h} = -\nabla\psi - \boldsymbol{\mu}$ implies that $\boldsymbol{\sigma} = -\frac{1}{2}\mathsf{I}\nabla\cdot\mathbf{h} + \frac{1}{2}\boldsymbol{\epsilon}\operatorname{curl}\mathbf{h} + \boldsymbol{\sigma}^{(s)}$ [*check*], and

$$\sigma_{pq} = \varepsilon_{pr}\partial_r(-\varepsilon_{qs}h_s). \tag{48}$$

In this sense, $\mathbf{h}$ can be regarded as a vector potential for the force stress, and ψ and Ψ can be regarded as scalar potentials of $\mathbf{h}$ in a Helmholtz decomposition ($\mathbf{h}$ being the sum of a gradient of ψ and a curl of Ψ).

The gradient of a smooth deformation $\mathbf{u}(\mathbf{x})$ can be decomposed into $\mathsf{E} + \mathsf{W}$, where $\mathsf{E} = \mathsf{E}^\top \equiv \frac{1}{2}(\nabla\mathbf{u} + \nabla\mathbf{u}^\top)$ represents strain and $\mathsf{W} \equiv \frac{1}{2}(\nabla\mathbf{u} - \nabla\mathbf{u}^\top) = \boldsymbol{\varepsilon}\omega$ is a rotation, where $\omega \equiv \frac{1}{2}\nabla\cdot(\boldsymbol{\varepsilon}\mathbf{u})$. Likewise, $\mathsf{M} \equiv (\nabla\otimes\nabla)\mathbf{u}$ can be deomposed as $\mathsf{M} = \nabla\mathsf{E} + \nabla\mathsf{W}$. M is symmetric in its first two arguments, while contracting over them gives

$$\mathsf{I} : \nabla\mathsf{W} = \tfrac{1}{2}(\nabla^2\mathbf{u} - \nabla(\nabla\cdot\mathbf{u})) \equiv -2\boldsymbol{\kappa}, \tag{49}$$

which defines a curvature vector $\boldsymbol{\kappa}$ [20]. The corresponding principle of virtual work for a continuous couple-stress material occupying a volume $\mathcal{V}$ can then be written [20]

$$\int_{\mathcal{V}} \left(\boldsymbol{\sigma}^{(s)} : \delta\mathsf{E} - 2\boldsymbol{\mu}\cdot\delta\boldsymbol{\kappa}\right) \mathrm{d}V = \int_{\partial\mathcal{V}} (\boldsymbol{\tau}\cdot\delta\mathbf{u} + m\delta\omega)\ \mathrm{d}S, \tag{50}$$

showing that the curvature vector is energy-conjugate to the couple-stress vector. Here $\boldsymbol{\tau} = \mathbf{n}\cdot\boldsymbol{\sigma}$ is a force traction at a surface with unit normal $\mathbf{n}$, and $m = \mathbf{n}\cdot\boldsymbol{\varepsilon}\boldsymbol{\mu}$ is a couple traction. Below, we seek the discrete analogues of (44, 50) for a confluent monolayer of polygonal cells.

B Discrete operators in 2D

The discrete analogues of differential operators appear in a variety of forms, being defined over primal and dual networks and acting on variables defined on vertices, edges, and faces of each [18]. These are summarised in Fig. 2, which shows the primary operators on the cell network (grad^v, curl^v, curl^c and div^c) and on the dual network (grad^c, CURL^v, CURL^c and div^v).

B.1 Operators on the primary network

We define vector spaces $\mathcal{V}$, $\mathcal{E}$, $\mathcal{F}$ of fields defined on vertices, edges and faces, with associated inner products $[\cdot,\cdot]_\mathcal{V}$, $[\cdot,\cdot]_\mathcal{E}$, $[\cdot,\cdot]_\mathcal{F}$, represented by matrices $\mathsf{M}^\mathcal{V}$, $\mathsf{M}^\mathcal{E}$, $\mathsf{M}^\mathcal{F}$. Thus

$$[\phi,\psi]_\mathcal{V} \equiv \textstyle\sum_{k,k'}\phi_k M^\mathcal{V}_{kk'}\psi_{k'}, \quad [\mathbf{u},\mathbf{v}]_\mathcal{E} \equiv \textstyle\sum_{j,j'}\mathbf{u}_j^\top \mathsf{M}^\mathcal{E}_{jj'}\mathbf{v}_{j'}, \quad [f,g]_\mathcal{F} \equiv \textstyle\sum_{i,i'} f_i M^\mathcal{F}_{ii'} g_{i'} \tag{51}$$

for any $\phi,\psi\in\mathcal{V}$, $\mathbf{u},\mathbf{v}\in\mathcal{E}$, $f,g\in\mathcal{F}$ (typically, we consider vectors defined on edges and scalars on vertices and faces). We reserve bold font for vectors in $\mathbb{R}^2$. Below we will assume that

$$\mathsf{M}^\mathcal{V} = \mathrm{diag}(E_k), \quad \mathsf{M}^\mathcal{E} = \mathrm{diag}(\mathsf{I}F_j), \quad \mathsf{M}^\mathcal{F} = \mathrm{diag}(A_i). \tag{52}$$

$\mathsf{M}^\mathcal{E}$ is chosen to have dimensions of area and to be symmetric between edges and links. The total monolayer area satisfies $\mathcal{A} = \sum_i A_i = \frac{1}{2}\sum_j F_j = \sum_k E_k$. I in (52) is the 2×2 identity.

The 'primary operators' over cells are $\mathrm{grad}^v : \mathcal{V}\to\mathcal{E}$, $\mathrm{curl}^v : \mathcal{V}\to\mathcal{E}$, $\mathrm{curl}^c : \mathcal{E}\to\mathcal{F}$ and $\mathrm{div}^c : \mathcal{E}\to\mathcal{F}$, and are defined by

$$\{\mathrm{grad}^v\,\phi\}_j = \textstyle\sum_k A_{jk}\frac{\mathbf{t}_j}{t_j^2}\phi_k, \qquad \{\mathrm{curl}^c\,\mathbf{b}\}_i = \frac{1}{A_i}\sum_j B_{ij}\mathbf{t}_j\cdot\mathbf{b}_j, \tag{53a}$$

$$\{\mathrm{curl}^v\phi\}_j = \textstyle\sum_k \frac{\boldsymbol{\epsilon}_k\mathbf{t}_j}{t_j^2}A_{jk}\phi_k, \qquad \{\mathrm{div}^c\,\mathbf{b}\}_i = -\frac{1}{A_i}\sum_j B_{ij}(\boldsymbol{\epsilon}_i\mathbf{t}_j)\cdot\mathbf{b}_j, \tag{53b}$$

We can write these in matrix form as

$$\mathrm{grad}^v = (\mathsf{N}^\mathcal{E})^{-1}\mathsf{A}\mathsf{N}^\mathcal{V}, \qquad \mathrm{curl}^c = (\mathsf{N}^\mathcal{F})^{-1}\mathsf{B}\mathsf{N}^\mathcal{E}, \tag{54a}$$

$$\mathrm{curl}^v = (\tilde{\mathsf{N}}^\mathcal{E})^{-1}\mathsf{A}\mathsf{N}^\mathcal{V}, \qquad \mathrm{div}^c = (\mathsf{N}^\mathcal{F})^{-1}\mathsf{B}\tilde{\mathsf{N}}^\mathcal{E}, \tag{54b}$$

where $\mathsf{N}^\mathcal{V}=\mathsf{I}$, $\mathsf{N}^\mathcal{E}=\mathrm{diag}(\mathbf{t}_j^\top)$, $\mathsf{N}^\mathcal{F}=\mathrm{diag}(A_i)$ and $\tilde{\mathsf{N}}^\mathcal{E}=\mathrm{diag}(-(\boldsymbol{\epsilon}_i\mathbf{t}_j)^\top)$ (so $(\mathsf{N}^\mathcal{E})^{-1}=\mathrm{diag}(\mathbf{t}_j/t_j^2)$, $(\tilde{\mathsf{N}}^\mathcal{E})^{-1} = \mathrm{diag}((\boldsymbol{\epsilon}_k\mathbf{t}_j)/t_j^2)$). The topological relationship $\mathsf{BA}=\mathsf{0}$ ensures that $\mathrm{curl}^c\circ\mathrm{grad}^v = 0$ and $\mathrm{div}^c\circ\mathrm{curl}^v = 0$. These exact sequences (de Rahm complexes) can be represented using the commutative diagrams

$$\begin{array}{ccccc} \mathcal{V} & \xrightarrow{\mathrm{grad}^v} & \mathcal{E} & \xrightarrow{\mathrm{curl}^c} & \mathcal{F} \\ \downarrow{\scriptstyle \mathsf{N}^\mathcal{V}} & & \downarrow{\scriptstyle \mathsf{N}^\mathcal{E}} & & \downarrow{\scriptstyle \mathsf{N}^\mathcal{F}} \\ \mathcal{V} & \xrightarrow{\mathsf{A}} & \mathcal{E} & \xrightarrow{\mathsf{B}} & \mathcal{F} \end{array} \quad\text{and}\quad \begin{array}{ccccc} \mathcal{V} & \xrightarrow{\mathrm{curl}^v} & \mathcal{E} & \xrightarrow{\mathrm{div}^c} & \mathcal{F} \\ \downarrow{\scriptstyle \mathsf{N}^\mathcal{V}} & & \downarrow{\scriptstyle \tilde{\mathsf{N}}^\mathcal{E}} & & \downarrow{\scriptstyle \mathsf{N}^\mathcal{F}} \\ \mathcal{V} & \xrightarrow{\mathsf{A}} & \mathcal{E} & \xrightarrow{\mathsf{B}} & \mathcal{F} \end{array} . \tag{55}$$

The left-hand sequence generates vectors oriented tangentially to edges; the right-hand sequence generates vectors oriented normally to edges. [*Check for transposes in curls.*]

Adjoints of the primary operators (denoted with $*$) under inner products (51) satisfy

$$[\mathrm{grad}^v\,\phi,\mathbf{b}]_\mathcal{E} = [\phi,\mathrm{grad}^{v*}\,\mathbf{b}]_\mathcal{V}, \qquad [\mathrm{curl}^c\,\mathbf{b},f]_\mathcal{F} = [\mathbf{b},\mathrm{curl}^{c*}f]_\mathcal{E}, \tag{56a}$$

$$[\mathrm{curl}^v\,\phi,\mathbf{b}]_\mathcal{E} = [\phi,\mathrm{curl}^{v*}\,\mathbf{b}]_\mathcal{V}, \qquad [\mathrm{div}^c\,\mathbf{b},f]_\mathcal{F} = [\mathbf{b},\mathrm{div}^{c*}f]_\mathcal{E}, \tag{56b}$$

for any $\phi\in\mathcal{V}$, $\mathbf{b}\in\mathcal{E}$, $f\in\mathcal{F}$. Derived operators (denoted with tildes, following the terminology and approach of [21]) are defined in terms of adjoint operators by

$$\widetilde{\mathrm{grad}}^c = -\mathrm{div}^{c*}, \quad \widetilde{\mathrm{curl}}^v = \mathrm{curl}^{v*}, \quad \widetilde{\mathrm{curl}}^c = \mathrm{curl}^{c*}, \quad \widetilde{\mathrm{div}}^v = -\mathrm{grad}^{v*}. \tag{57}$$

It follows from (51, 56) that the derived operators have the following matrix representations:

$$\widetilde{\mathrm{grad}}^c = -(\mathsf{M}^\mathcal{E})^{-1}\mathrm{div}^{c\top}\mathsf{M}^\mathcal{F}, \qquad \widetilde{\mathrm{curl}}^c = (\mathsf{M}^\mathcal{E})^{-1}\mathrm{curl}^{c\top}\mathsf{M}^\mathcal{F}, \tag{58a}$$

$$\widetilde{\mathrm{curl}}^v = (\mathsf{M}^\mathcal{V})^{-1}\mathrm{curl}^{v\top}\mathsf{M}^\mathcal{E}, \qquad \widetilde{\mathrm{div}}^v = -(\mathsf{M}^\mathcal{V})^{-1}\mathrm{grad}^{v\top}\mathsf{M}^\mathcal{E}. \tag{58b}$$

These relationships can be summarised as follows:

$$\begin{array}{ccccc} \mathcal{V} & \xrightarrow{\mathrm{grad}^v} & \mathcal{E} & \xrightarrow{\mathrm{curl}^c} & \mathcal{F} \\ \uparrow{\scriptstyle \mathsf{M}^{\mathcal{V}}} & & \uparrow{\scriptstyle \mathsf{M}^{\mathcal{E}}} & & \uparrow{\scriptstyle \mathsf{M}^{\mathcal{F}}} \\ \mathcal{V} & \xleftarrow[-\widetilde{\mathrm{div}}^v]{} & \mathcal{E} & \xleftarrow[\widetilde{\mathrm{curl}}^c]{} & \mathcal{F} \end{array} \quad \text{and} \quad \begin{array}{ccccc} \mathcal{V} & \xrightarrow{\mathrm{curl}^v} & \mathcal{E} & \xrightarrow{\mathrm{div}^c} & \mathcal{F} \\ \uparrow{\scriptstyle \mathsf{M}^{\mathcal{V}}} & & \uparrow{\scriptstyle \mathsf{M}^{\mathcal{E}}} & & \uparrow{\scriptstyle \mathsf{M}^{\mathcal{F}}} \\ \mathcal{V} & \xleftarrow[\widetilde{\mathrm{curl}}^v]{} & \mathcal{E} & \xleftarrow[-\widetilde{\mathrm{grad}}^c]{} & \mathcal{F} \end{array} . \tag{59}$$

Under (58), $\widetilde{\mathrm{div}}^v \circ \widetilde{\mathrm{curl}}^c = 0$ and $\widetilde{\mathrm{curl}}^v \circ \widetilde{\mathrm{grad}}^c = 0$ are both satisfied exactly: for example,

$$\begin{aligned} -\widetilde{\mathrm{div}}^v \circ \widetilde{\mathrm{curl}}^c =& (\mathsf{M}^{\mathcal{V}})^{-1}(\mathrm{grad}^v)^\top \mathsf{M}^{\mathcal{E}} \circ (\mathsf{M}^{\mathcal{E}})^{-1}(\mathrm{curl}^c)^\top \mathsf{M}^{\mathcal{F}} \\ =& (\mathsf{M}^{\mathcal{V}})^{-1}((\mathsf{N}^{\mathcal{E}})^{-1}\mathsf{A}\mathsf{N}^{\mathcal{V}})^\top ((\mathsf{N}^{\mathcal{F}})^{-1}\mathsf{B}\mathsf{N}^{\mathcal{E}})^\top \mathsf{M}^{\mathcal{F}} \\ =& (\mathsf{M}^{\mathcal{V}})^{-1}(\mathsf{N}^{\mathcal{V}})^\top \mathsf{A}^\top \mathsf{B}^\top ((\mathsf{N}^{\mathcal{F}})^{-1})^\top \mathsf{M}^{\mathcal{F}}, \end{aligned} \tag{60}$$

which vanishes because $(\mathsf{B}\mathsf{A})^\top = \mathsf{0}$. The sequences in (58c) are therefore 'exact.'

Derived operators under the choice of inner product (51) are

$$\{\widetilde{\mathrm{grad}}^c f\}_j = \textstyle\sum_i B_{ij} \dfrac{(\boldsymbol{\epsilon}_i \mathbf{t}_j)}{F_j} f_i, \qquad \{\widetilde{\mathrm{curl}}^c f\}_j = \textstyle\sum_i B_{ij} \dfrac{\mathbf{t}_j}{F_j} f_i, \tag{61a}$$

$$\{\widetilde{\mathrm{curl}}^v \mathbf{b}\}_k = \frac{1}{E_k} \textstyle\sum_j A_{jk} \dfrac{F_j}{t_j^2} (\boldsymbol{\epsilon}_k \mathbf{t}_j) \cdot \mathbf{b}_j, \qquad \{\widetilde{\mathrm{div}}^v \mathbf{b}\}_k = -\frac{1}{E_k} \textstyle\sum_j A_{jk} \dfrac{F_j}{t_j^2} \mathbf{t}_j \cdot \mathbf{b}_j. \tag{61b}$$

It follows from (61) that grad^v and $\widetilde{\mathrm{curl}}^c$ are both parallel to $\mathbf{t}_j$ and curl^v and $\widetilde{\mathrm{grad}}^c$ are both parallel to $\boldsymbol{\epsilon}_i \mathbf{t}_j$.

By specifying fields appropriately in (56), we can write, for any $\phi \in \mathcal{V}$, $\mathbf{b} \in \mathcal{E}$ and $f \in \mathcal{V}$,

$$0 \leq [\mathrm{grad}^v \phi, \mathrm{grad}^v \phi]_{\mathcal{E}} = [\phi, -\widetilde{\mathrm{div}}^v \circ \mathrm{grad}^v \phi]_{\mathcal{V}}, \qquad 0 \leq [\mathrm{curl}^c \mathbf{b}, \mathrm{curl}^c \mathbf{b}]_{\mathcal{F}} = [\mathbf{b}, \widetilde{\mathrm{curl}}^c \circ \mathrm{curl}^c \mathbf{b}]_{\mathcal{E}}, \tag{62a}$$

$$0 \leq [\mathrm{curl}^v \phi, \mathrm{curl}^v \phi]_{\mathcal{E}} = [\phi, \widetilde{\mathrm{curl}}^v \circ \mathrm{curl}^v \phi]_{\mathcal{V}}, \qquad 0 \leq [\mathrm{div}^c \mathbf{b}, \mathrm{div}^c \mathbf{b}]_{\mathcal{F}} = [\mathbf{b}, -\widetilde{\mathrm{grad}}^c \circ \mathrm{div}^c \mathbf{b}]_{\mathcal{E}}, \tag{62b}$$

$$0 \leq [\widetilde{\mathrm{grad}}^c f, \widetilde{\mathrm{grad}}^c f]_{\mathcal{E}} = [f, -\mathrm{div}^c \circ \widetilde{\mathrm{grad}}^c f]_{\mathcal{F}}, \qquad 0 \leq [\widetilde{\mathrm{curl}}^v \mathbf{b}, \widetilde{\mathrm{curl}}^v \mathbf{b}]_{\mathcal{V}} = [\mathbf{b}, \mathrm{curl}^v \circ \widetilde{\mathrm{curl}}^v \mathbf{b}]_{\mathcal{E}}, \tag{62c}$$

$$0 \leq [\widetilde{\mathrm{curl}}^c f, \widetilde{\mathrm{curl}}^c f]_{\mathcal{E}} = [f, \mathrm{curl}^c \circ \widetilde{\mathrm{curl}}^c f]_{\mathcal{F}}, \qquad 0 \leq [\widetilde{\mathrm{div}}^v \mathbf{b}, \widetilde{\mathrm{div}}^v \mathbf{b}]_{\mathcal{V}} = [\mathbf{b}, -\mathrm{grad}^v \circ \widetilde{\mathrm{div}}^v \mathbf{b}]_{\mathcal{E}}. \tag{62d}$$

This construction identifies two positive-semi-definite scalar Laplacians acting on $\mathcal{V}$,

$$-\widetilde{\mathrm{div}}^v \circ \mathrm{grad}^v = (\mathsf{M}^{\mathcal{V}})^{-1}(\mathsf{N}^{\mathcal{V}})^\top \mathsf{A}^\top (\mathsf{N}^{\mathcal{E}})^{-1,\top} \mathsf{M}^{\mathcal{E}} (\mathsf{N}^{\mathcal{E}})^{-1} \mathsf{A}\mathsf{N}^{\mathcal{V}} \tag{63a}$$

$$\widetilde{\mathrm{curl}}^v \circ \mathrm{curl}^v = (\mathsf{M}^{\mathcal{V}})^{-1}(\mathsf{N}^{\mathcal{V}})^\top \mathsf{A}^\top (\tilde{\mathsf{N}}^{\mathcal{E}})^{-1,\top} \mathsf{M}^{\mathcal{E}} (\tilde{\mathsf{N}}^{\mathcal{E}})^{-1} \mathsf{A}\mathsf{N}^{\mathcal{V}}, \tag{63b}$$

which differ in having at their heart $\hat{\mathbf{t}}_j^\top \{\mathsf{M}^{\mathcal{E}}\}_{jj} \hat{\mathbf{t}}_j$ and $(-\boldsymbol{\epsilon}_i \hat{\mathbf{t}}_j)^\top \{\mathsf{M}^{\mathcal{E}}\}_{jj} (-\boldsymbol{\epsilon}_k \hat{\mathbf{t}}_j)$. Taking $\mathsf{M}^{\mathcal{E}} = \mathrm{diag}(\mathsf{I}F_j)$ recovers $\mathsf{L}_{\mathcal{V}}$ (see (8a)) in each case in (63). There are two positive-semi-definite scalar Laplacians acting on $\mathcal{F}$, which for $\mathsf{M}^{\mathcal{E}} = \mathrm{diag}(\mathsf{I}F_j)$ reduce to

$$-\mathrm{div}^c \circ \widetilde{\mathrm{grad}}^c = \mathsf{L}_{\mathcal{F}}, \quad \mathrm{curl}^c \circ \widetilde{\mathrm{curl}}^c = \mathsf{L}_{\mathcal{F}}. \tag{63c}$$

We can also use (56) to obtain the orthogonality relations

$$[\mathrm{grad}^v \phi, \widetilde{\mathrm{curl}}^c f]_{\mathcal{E}} = 0 \quad \text{and} \quad [\mathrm{curl}^v \phi, \widetilde{\mathrm{grad}}^c f]_{\mathcal{E}} = 0, \tag{64}$$

which hold for any functions $\phi \in \mathcal{V}$ and $f \in \mathcal{F}$. These results rely on $\mathsf{B}\mathsf{A} = \mathsf{0}$, rather than geometric orthogonality. This leads to the decomposition given in (9).

We also identify two Helmholtzians (closely related to Hodge Laplacians $\mathsf{A}\mathsf{A}^\top + \mathsf{B}^\top \mathsf{B}$) acting on $\mathcal{E}$,

$$\mathcal{H}_1 = \widetilde{\mathrm{curl}}^c \circ \mathrm{curl}^c - \widetilde{\mathrm{grad}}^v \circ \mathrm{div}^v, \tag{65a}$$

$$\mathcal{H}_2 = \mathrm{curl}^v \circ \widetilde{\mathrm{curl}}^v - \mathrm{grad}^c \circ \widetilde{\mathrm{div}}^c, \tag{65b}$$

which sit in the spaces spanned by $\hat{\mathbf{t}}_j \otimes \hat{\mathbf{t}}_j$ and $(\boldsymbol{\epsilon}_k\hat{\mathbf{t}}_j) \otimes (\boldsymbol{\epsilon}_k\hat{\mathbf{t}}_j)$ respectively. We assume that $\dim(\ker(\mathcal{H}_1)) = 0$ and $\dim(\ker(\mathcal{H}_2)) = 0$, ensuring that there are no additional harmonic contributions to the decomposition (9). A necessary condition is that the domain has no holes [33]. In this case, $\ker(\text{curl}^c) = \text{im}(\text{grad}^v)$, $\ker(\text{div}^c) = \text{im}(\text{curl}^v)$, with analogous results for derived operators [21], ensuring sequences (59) are exact.

B.2 Operators on the dual network

Primary operators on the dual network are defined as follows:

$$\begin{array}{ccccc} \mathcal{T} & \xleftarrow{\text{CURL}^v} & \mathcal{L} & \xleftarrow{\text{grad}^c} & \mathcal{C} \\ \downarrow{\scriptstyle \mathsf{N}^{\mathcal{T}}} & & \downarrow{\scriptstyle \mathsf{N}^{\mathcal{L}}} & & \downarrow{\scriptstyle \mathsf{N}^{\mathcal{C}}} \\ \mathcal{T} & \xleftarrow{\mathsf{A}^\top} & \mathcal{L} & \xleftarrow{\mathsf{B}^\top} & \mathcal{C} \end{array} \quad \text{and} \quad \begin{array}{ccccc} \mathcal{T} & \xleftarrow{\text{div}^v} & \mathcal{L} & \xleftarrow{\text{CURL}^c} & \mathcal{C} \\ \downarrow{\scriptstyle \mathsf{N}^{\mathcal{T}}} & & \downarrow{\scriptstyle \tilde{\mathsf{N}}^{\mathcal{L}}} & & \downarrow{\scriptstyle \mathsf{N}^{\mathcal{C}}} \\ \mathcal{T} & \xleftarrow{\mathsf{A}^\top} & \mathcal{L} & \xleftarrow{\mathsf{B}^\top} & \mathcal{C} \end{array} \quad . \tag{66}$$

Here $\mathsf{N}^{\mathcal{C}} = \mathsf{I}$, $\mathsf{N}^{\mathcal{L}} = \text{diag}(\mathbf{T}_j^\top)$, $\tilde{\mathsf{N}}^{\mathcal{L}} = \text{diag}(-(\boldsymbol{\epsilon}_k\mathbf{T}_j)^\top)$, $\mathsf{N}^{\mathcal{T}} = \text{diag}(E_k)$. $\mathcal{T}$, $\mathcal{L}$ and $\mathcal{C}$ are vector spaces of fields defined over triangles, links and cell centres. We can make the association $\mathcal{T} = \mathcal{V}$, $\mathcal{L} = \mathcal{E}$, $\mathcal{C} = \mathcal{F}$ (subject to boundary effects). Derived operators are defined using the inner products with metrics $\mathsf{M}^{\mathcal{T}} = \mathsf{M}^{\mathcal{V}}$, $\mathsf{M}^{\mathcal{L}} = \mathsf{M}^{\mathcal{E}}$, $\mathsf{M}^{\mathcal{C}} = \mathsf{M}^{\mathcal{F}}$, via

$$\begin{array}{ccccc} \mathcal{T} & \xleftarrow{\text{CURL}^v} & \mathcal{L} & \xleftarrow{\text{grad}^c} & \mathcal{C} \\ \uparrow{\scriptstyle \mathsf{M}^{\mathcal{T}}} & & \uparrow{\scriptstyle \mathsf{M}^{\mathcal{L}}} & & \uparrow{\scriptstyle \mathsf{M}^{\mathcal{C}}} \\ \mathcal{T} & \xrightarrow[\widetilde{\text{CURL}}^v]{} & \mathcal{L} & \xrightarrow[-\widetilde{\text{div}}^c]{} & \mathcal{C} \end{array} \quad \text{and} \quad \begin{array}{ccccc} \mathcal{T} & \xleftarrow{\text{div}^v} & \mathcal{L} & \xleftarrow{\text{CURL}^c} & \mathcal{C} \\ \uparrow{\scriptstyle \mathsf{M}^{\mathcal{T}}} & & \uparrow{\scriptstyle \mathsf{M}^{\mathcal{L}}} & & \uparrow{\scriptstyle \mathsf{M}^{\mathcal{C}}} \\ \mathcal{T} & \xrightarrow[-\widetilde{\text{grad}}^v]{} & \mathcal{L} & \xrightarrow[\widetilde{\text{CURL}}^c]{} & \mathcal{C} \end{array} \quad . \tag{67}$$

Thus

$$\{\text{grad}^c f\}_j = \textstyle\sum_i B_{ij}\dfrac{\mathbf{T}_j}{T_j^2}f_i, \qquad \{\text{CURL}^v \mathbf{b}\}_k = \dfrac{1}{E_k}\textstyle\sum_j A_{jk}\mathbf{T}_j \cdot \mathbf{b}_j, \tag{68a}$$

$$\{\text{CURL}^c f\}_j = \textstyle\sum_k \dfrac{\boldsymbol{\epsilon}_i\mathbf{T}_j}{T_j^2}B_{ij}f_i, \qquad \{\text{div}^v \mathbf{b}\}_k = -\dfrac{1}{E_k}\textstyle\sum_j A_{jk}(\boldsymbol{\epsilon}_k\mathbf{T}_j) \cdot \mathbf{b}_j \tag{68b}$$

and [*check signs, transposes*]

$$\{\widetilde{\text{grad}}^v\,\phi\}_j = \textstyle\sum_k A_{jk}\dfrac{(\boldsymbol{\epsilon}_k\mathbf{T}_j)}{F_j}\phi_k \qquad \{\widetilde{\text{CURL}}^v\,\phi\}_j = \dfrac{1}{F_j}\textstyle\sum_j A_{jk}\mathbf{T}_j\phi_k \tag{69a}$$

$$\{\widetilde{\text{CURL}}^c\,\mathbf{b}\}_i = \dfrac{1}{E_k}\textstyle\sum_j B_{ij}\dfrac{F_j}{T_j}^2(\boldsymbol{\epsilon}_i\mathbf{T}_j) \cdot \mathbf{b}_j \qquad \{\widetilde{\text{div}}^c\,\mathbf{b}\}_i = -\dfrac{1}{A_i}\textstyle\sum_j B_{ij}\dfrac{F_j}{T_j^2}\mathbf{T}_j \cdot \mathbf{b}_j \tag{69b}$$

[*Check the operation of derived operators at exterior vertices and edges.*]

The primary and derived operators over the two networks then act as shown below:

$$\begin{array}{ccc} \mathcal{V} & \xleftarrow{\mathsf{M}^{\mathcal{V}}} & \mathcal{V} \\ {\scriptstyle \text{curl}^v}\downarrow\ \uparrow{\scriptstyle -\widetilde{\text{div}}^v} & & {\scriptstyle \widetilde{\text{curl}}^v}\uparrow\ \downarrow{\scriptstyle \text{grad}^v} \\ \mathcal{E} & \xleftarrow{\mathsf{M}^{\mathcal{E}}} & \mathcal{E} \\ {\scriptstyle \text{div}^c}\downarrow\ \uparrow{\scriptstyle \widetilde{\text{curl}}^c} & & {\scriptstyle -\widetilde{\text{grad}}^c}\uparrow\ \downarrow{\scriptstyle \text{curl}^c} \\ \mathcal{F} & \xleftarrow{\mathsf{M}^{\mathcal{F}}} & \mathcal{F} \end{array} \qquad \begin{array}{ccc} \mathcal{T} & \xleftarrow{\mathsf{M}^{\mathcal{T}}} & \mathcal{T} \\ {\scriptstyle \text{CURL}^v}\uparrow\ \downarrow{\scriptstyle \text{div}^v} & & {\scriptstyle \widetilde{\text{CURL}}^v}\downarrow\ \uparrow{\scriptstyle -\widetilde{\text{grad}}^v} \\ \mathcal{L} & \xleftarrow{\mathsf{M}^{\mathcal{L}}} & \mathcal{L} \\ {\scriptstyle \text{grad}^c}\uparrow\ \downarrow{\scriptstyle \text{CURL}^c} & & {\scriptstyle -\widetilde{\text{div}}^c}\downarrow\ \uparrow{\scriptstyle \widetilde{\text{CURL}}^c} \\ \mathcal{C} & \xleftarrow{\mathsf{M}^{\mathcal{C}}} & \mathcal{C} \end{array} \quad . \tag{70}$$

This leads to the Helmholtz decomposition given in (11).

B.3 Operators acting on tensors

Divergence of quantities $\boldsymbol{\sigma}$ defined on vertices or cell centres is given by

$$\{\mathrm{div}^c \boldsymbol{\sigma}^c\} = \textstyle\sum_j \boldsymbol{\epsilon}_i^\top B_{ij} \mathbf{t}_j \cdot \boldsymbol{\sigma}_i / A_i = A_i^{-1} \sum_j \mathbf{n}_{ij} \cdot \boldsymbol{\sigma}_i \tag{71a}$$

$$\{\mathrm{div}^v \boldsymbol{\sigma}^v\} = \textstyle\sum_j \boldsymbol{\epsilon}_k^\top A_{jk} \mathbf{T}_j \cdot \boldsymbol{\sigma}_k / E_k = E_k^{-1} \sum_j \mathbf{N}_{jk} \cdot \boldsymbol{\sigma}_k \tag{71b}$$

Divergence maps from cells/faces to links/edges [*not clear via notation*].

B.4 Inverting Laplacians

We note that $\mathsf{L}_\mathcal{V}$ satisfies

$$[\phi, \mathsf{L}_\mathcal{V} \phi]_\mathcal{V} \equiv \phi^\top \mathsf{E} \mathsf{L}_\mathcal{V} \phi \geq 0. \tag{72}$$

Noting that $\mathsf{E}^\top = \mathsf{E}$ and $\mathsf{L}_\mathcal{V} = \mathsf{E}^{-1} \mathsf{L}_\mathcal{V}^\top \mathsf{E}$, self-adjointness is demonstrated as follows:

$$[\phi, \mathsf{L}_\mathcal{V} \psi]_\mathcal{V} = \phi^\top \mathsf{E} \mathsf{L}_\mathcal{V} \psi = \psi^\top \mathsf{L}_\mathcal{V}^\top \mathsf{E} \phi = \psi^\top \mathsf{E} \mathsf{E}^{-1} \mathsf{L}_\mathcal{V}^\top \mathsf{E} \phi = \psi^\top \mathsf{E} \mathsf{L}_\mathcal{V} \phi = [\psi, \mathsf{L}_\mathcal{V} \phi]_\mathcal{V}. \tag{73}$$

Let λ_k and e_k ($k = 1, \ldots, \lambda_{N_v}$) be the eigenvalues and eigenvectors of $\mathsf{L}_\mathcal{V}$. Then

$$[e_p, \mathsf{L}_\mathcal{V} e_q]_\mathcal{V} = \lambda_q [e_p, e_q]_\mathcal{V} = [\mathsf{L}_\mathcal{V} e_p, e_q]_\mathcal{V} = \lambda_p [e_p, e_q]_\mathcal{V} \tag{74}$$

and so $(\lambda_q - \lambda_p)[e_p, e_q]_\mathcal{V} = 0$, demonstrating orthogonality (under the inner product) of eigenvectors having distinct eigenvalues. Writing $\phi = \sum_k c_k e_k$ and projecting onto $\mathbf{e}_p$, it follows that

$$\phi = \textstyle\sum_k \dfrac{[e_k, \phi]_\mathcal{V}}{[e_k, e_k]_\mathcal{V}} e_k. \tag{75}$$

We expect that $\lambda_1 = 0$ and $e_1 = \mathbb{1}$, with remaining eigenvalues being positive. To invert $\mathsf{L}_\mathcal{V} \phi = g$, we define $\overline{g} \equiv [e_1, g]_\mathcal{V} \mathbb{1} / N_v$ and set $\hat{g} \equiv g - \overline{g}$. Then write $\phi = \overline{\phi} + \hat{\phi}$ where

$$\mathsf{L}_\mathcal{V} \overline{\phi} = \overline{g}, \quad \mathsf{L}_\mathcal{V} \hat{\phi} = \hat{g}. \tag{76}$$

The former equation has the solution $\overline{\phi} = ([e_1, g]_\mathcal{V} / N_v) \overline{\phi}_0$ where $\mathsf{L}_\mathcal{V} \overline{\phi}_0 = \mathbb{1}$, while the latter equation satisfies the solvability condition $[\mathbf{e}_1, \hat{g}] = 0$. We can project this equation onto the remaining eigenmodes, to obtain

$$\phi = \frac{[\mathbb{1}, g]_\mathcal{V}}{N_v} \overline{\phi}_0 + \sum_{k=2}^{N_v} \frac{1}{\lambda_k} \frac{[e_k, \hat{g}]_\mathcal{V}}{[e_k, e_k]_\mathcal{V}} e_k \tag{77}$$

Similar arguments follow for $\mathsf{L}_\mathcal{T}$ under $[\cdot, \cdot]_\mathcal{V}$, and $\mathsf{L}_\mathcal{C}$ and $\mathsf{L}_\mathcal{C}$ under $[\cdot, \cdot]_\mathcal{F}$.

C Changes of area and perimeter under non-uniform deformations

Here we consider how area and perimeter change under deformations $\mathbf{u}(\mathbf{x})$ that vary with position, over length-scales long compared to an individual cell. Dropping third (and higher) spatial derivatives of $\mathbf{u}$, edges, edge lengths and normals map under the deformation to

$$\mathbf{t}_j \equiv \textstyle\sum_k A_{jk} \mathbf{r}_k = \mathbf{t}'_j + \sum_k A_{jk} \mathbf{u}(\mathbf{r}'_k) = \mathbf{t}'_j + \mathbf{t}'_j \cdot (\nabla \mathbf{u})_j + \ldots, \tag{78a}$$

$$t_j \equiv \sqrt{\mathbf{t}_j \cdot \mathbf{t}_j} = t'_j \left[1 + \hat{\mathbf{t}}'_j \cdot \mathsf{E}_j \cdot \hat{\mathbf{t}}'_j + \ldots\right], \tag{78b}$$

$$\mathbf{n}_{ij} \equiv -\boldsymbol{\epsilon}_i B_{ij} \mathbf{t}_j = \mathbf{n}'_{ij} + \mathbf{n}'_{ij} \cdot (\nabla \mathbf{u})_j + \cdots = \mathbf{n}'_{ij} \cdot \left[\mathsf{I} + (\nabla \mathbf{u})_i + \mathbf{v}'_{ij} \cdot \mathsf{M}_i\right] + \ldots, \tag{78c}$$

where (78c) shows how the mapping is referred to an adjacent cell centre. Here $\mathbf{v}_{ij}$ is the vector connecting cell centre $\mathbf{R}_i$ to an adjacent edge centroid $\mathbf{c}_j$, i.e. $\overline{B}_{ij}(\mathbf{c}_j - \mathbf{R}_i - \mathbf{v}_{ij}) = \mathbf{0}$. We define the cell centre to be

the centroid with respect to vertices, i.e. $\mathbf{R}_i = Z_i^{-1}\sum_k C_{ik}\mathbf{r}_k$. It is also the centroid relative to edge centroids (because $\sum_k C_{ik}\mathbf{r}_k = \frac{1}{2}\sum_{jk}\overline{B}_{ij}\overline{A}_{jk}\mathbf{r}_k = \sum_j \overline{B}_{ij}\mathbf{c}_j$, ensuring that $\sum_j \overline{B}_{ij}\mathbf{v}_{ij} = \mathbf{0}$). Likewise

$$\mathsf{E}_j = \mathsf{E}_i + \mathbf{v}'_{ij}\cdot(\nabla\mathsf{E})_i + \dots \tag{79}$$

Edge centroids map to

$$\mathbf{c}_j = \mathbf{c}'_j + \mathbf{u}_j + \tfrac{1}{8}(\mathbf{t}'_j\cdot\nabla)(\mathbf{t}'_j\cdot\nabla)\mathbf{u}|_j + \dots = \mathbf{c}'_j + \mathbf{u}_j + \tfrac{1}{8}(\mathbf{t}'_j\otimes\mathbf{t}'_j):\mathsf{M}_j + \dots. \tag{80}$$

Using $\mathbf{R}_i = Z_i^{-1}\sum_j \overline{B}_{ij}\mathbf{c}_j$, cell centres map to

$$\mathbf{R}_i = \mathbf{R}'_i + \mathbf{u}_i + \tfrac{1}{2}\mathsf{V}_i:\mathsf{M}_i + \tfrac{1}{8}\mathsf{T}_i:\mathsf{M}_i + \dots \tag{81}$$

where $\mathsf{V}_i \equiv Z_i^{-1}\sum_j \overline{B}_{ij}\mathbf{v}'_{ij}\otimes\mathbf{v}'_{ij}$ (arising from averaging displacements around the edges of the cell) and $\mathsf{T}_i \equiv Z_i^{-1}\sum_j \overline{B}_{ij}\mathbf{t}'_j\otimes\mathbf{t}'_j$. Combining (80) and (81), links from cell centres to edge centroids map to

$$\mathbf{v}_{ij} = \mathbf{v}'_{ij} + \mathbf{v}'_{ij}\cdot(\nabla\mathbf{u})_i + \left[\tfrac{1}{2}(\mathbf{v}'_{ij}\otimes\mathbf{v}'_{ij}) - \tfrac{1}{2}\mathsf{V}_i + \tfrac{1}{8}\overline{B}_{ij}(\mathbf{t}'_j\otimes\mathbf{t}'_j) - \tfrac{1}{8}\mathsf{T}_i\right]:\mathsf{M}_i + \dots \tag{82}$$

Using (80) and (78b), cell perimeters change according to

$$L_i \equiv \sum_j \overline{B}_{ij}t_j = L'_i(1+\mathsf{Q}_i:\mathsf{E}_i) + \textstyle\sum_j \overline{B}_{ij}t'_j\hat{\mathbf{t}}'_j\cdot\left[\mathbf{v}'_{ij}\cdot(\nabla\mathsf{E})_i\right]\cdot\hat{\mathbf{t}}'_j + \dots, \tag{83}$$

where $L'_i\mathsf{Q}_i \equiv \sum_j \overline{B}_{ij}\mathbf{t}'_j\otimes\hat{\mathbf{t}}'_j$. Writing the final term as $L'_i\mathsf{X}_i \vdots (\nabla\mathsf{E})_i$ reveals the 3-tensor X_i characterising the impact of strain gradients on cell perimeter. W does not affect perimeter changes to this order.

Using (78c) and (82), the cell area becomes

$$\begin{aligned}A_i \equiv& \tfrac{1}{2}\textstyle\sum_j \mathbf{n}_{ij}\cdot\mathbf{v}_{ij}\\ =& A'_i + \textstyle\sum_j\left\{\mathbf{v}'_{ij}\cdot\mathsf{E}_i\cdot\mathbf{n}'_{ij} + \tfrac{1}{2}\left[\mathbf{n}'_{ij}\cdot(\mathbf{v}'_{ij}\cdot\mathsf{M}_i)\right]\cdot\mathbf{v}'_{ij} + \tfrac{1}{2}\left(\left[\tfrac{1}{2}\mathbf{v}'_{ij}\otimes\mathbf{v}'_{ij} + \tfrac{1}{8}\overline{B}_{ij}\mathbf{t}'_j\otimes\mathbf{t}'_j - \tfrac{1}{2}\mathsf{V}_i - \tfrac{1}{8}\mathsf{T}_i\right]:\mathsf{M}_i\right)\cdot\mathbf{n}'_{ij}\right\}.\end{aligned}$$

Note that

$$\textstyle\sum_j \mathbf{n}_{ij}\otimes\mathbf{v}_{ij} = \sum_j \mathbf{n}_{ij}\otimes\mathbf{c}_{ij} = \oint_i \mathbf{x}\hat{\mathbf{n}}\,\mathrm{d}s = \int_i \nabla\mathbf{x}\,\mathrm{d}A = A_i\mathsf{I}. \tag{84}$$

A similar argument gives

$$\left(\textstyle\sum_j \mathbf{n}_{ij}\otimes\mathbf{v}_{ij}\otimes\mathbf{v}_{ij}\right)_{pqr} \equiv \sum_j n_{ij,p}v_{ij,q}v_{ij,r} = A_i\left[\delta_{pq}(\rho_{i,r}-R_{i,r}) + \delta_{pr}(\rho_{i,q}-R_{i,q}))\right] \tag{85}$$

where $\boldsymbol{\rho}_i \equiv A_i^{-1}\int_i \mathbf{x}\,\mathrm{d}A$ is the area-centroid of the cell, which in general will be distinct from the vertex centroid $\mathbf{R}_i$. Thus

$$\left[\mathbf{n}'_{ij}\cdot(\mathbf{v}'_{ij}\cdot\mathsf{M}_i)\right]\cdot\mathbf{v}'_{ij} = A'_i(\boldsymbol{\rho}'_i-\mathbf{R}'_i)\cdot[\nabla^2\mathbf{u}_i + \nabla(\nabla\cdot\mathbf{u}_i)] \equiv 2A'_i(\boldsymbol{\rho}'_i-\mathbf{R}'_i)\cdot[\mathsf{I}:\nabla\mathsf{E}]_i \tag{86a}$$

$$\left(\left[\mathbf{v}'_{ij}\otimes\mathbf{v}'_{ij}\right]:\mathsf{M}_i\right)\cdot\mathbf{n}'_{ij} = 2A'_i(\boldsymbol{\rho}'_i-\mathbf{R}'_i)\cdot\nabla(\nabla\cdot\mathbf{u}_i) \equiv 2A'_i(\boldsymbol{\rho}'_i-\mathbf{R}'_i)\cdot[\nabla(\mathsf{I}:\mathsf{E})]_i \tag{86b}$$

This gives

$$A_i = A'_i\left[1+\mathsf{I}:\mathsf{E}_i + (\boldsymbol{\rho}'_i-\mathbf{R}'_i)\cdot[\mathsf{I}:\nabla\mathsf{E}]_i + \tfrac{1}{2}(\boldsymbol{\rho}'_i-\mathbf{R}'_i)\cdot[\nabla(\mathsf{I}:\mathsf{E})]_i\right] + \tfrac{1}{2}\textstyle\sum_j\left(\left[\frac{1}{8}\overline{B}_{ij}\mathbf{t}'_j\otimes\mathbf{t}'_j\right]:\mathsf{M}_i\right)\cdot\mathbf{n}'_{ij}.$$

As $\mathbf{R}_i$ is the cell centroid (relative to vertices) then $\sum_j \mathbf{v}'_{ij} = \mathbf{0}$ and $\sum_j \mathbf{n}'_{ij} = \mathbf{0}$. [*Check: consider how a different choice of centroid eliminates the second and third terms.*] Then we note that

$$\begin{aligned}t_{j,p}t_{j,q}n_{ij,r}M_{pqr} =& -B_{ij}t_{j,p}t_{j,q}\epsilon_{i,rs}t_{j,s}(\partial_p E_{qr} + \partial_p W_{qr}) = -B_{ij}t_{j,p}t_{j,q}\epsilon_{i,rs}t_{j,s}(\partial_p E_{qr} + \partial_p\varepsilon_{qr}\omega_i)\\ =& \mp B_{ij}t_{j,p}t_{j,q}\varepsilon_{rs}t_{j,s}(\partial_p E_{qr} + \partial_p\varepsilon_{qr}\omega_i) = \mp B_{ij}t_{j,p}t_{j,q}t_{j,s}(\varepsilon_{rs}\partial_p E_{qr} - \delta_{qs}\partial_p\omega_i)\\ =& \mp B_{ij}t_{j,p}(t_{j,q}t_{j,s}\varepsilon_{rs}\partial_p E_{qr} - l_j^2\partial_p\omega_i) = \mp B_{ij}t_{j,p}t_{j,q}t_{j,s}\varepsilon_{rs}\partial_p E_{qr} + 2l_j^2\mathbf{n}_{ij}\cdot\boldsymbol{\kappa}_i\end{aligned} \tag{87}$$

taking $\boldsymbol{\epsilon}_i = \pm\boldsymbol{\varepsilon}$ and noting that $\mathbf{n}_{ij}\cdot\boldsymbol{\kappa}_i = \pm\frac{1}{2}B_{ij}t_{j,p}\partial_p\omega_i$.

Hence, with this constraint on cell centre location, we can write

$$A_i = A'_i\left[1+\mathsf{I}:\mathsf{E}_i + \mathsf{Y}_i\vdots(\nabla\mathsf{E})_i + \left[\frac{1}{8A'_i}\textstyle\sum_j\overline{B}_{ij}(t'_j)^2\mathbf{n}'_{ij}\right]\cdot\boldsymbol{\kappa}_i\right] \tag{88}$$

where Y_i has dimensions of length.

D Stress over the dual network

The energy in (35) is partitioned across cells, but it can be reoorganised to be partitioned over kites. The cell area A_i can be partitioned into kite areas K_{ik} so that $A_i = \sum_k K_{ik}$ and $\hat{E}_k = \sum_i K_{ik}$. The leading-order force-stress contribtution to the energy can be written

$$\textstyle\sum_i A_i \boldsymbol{\sigma}_i^{(s)} : \mathsf{E}_i \equiv \sum_i (A_i \mathcal{P}_i \mathsf{I} + \mathcal{T}_i L_i \mathsf{Q}_i) : \mathsf{E}_i = \sum_k \hat{E}_k \boldsymbol{\sigma}_k^{(s)} : \mathsf{E}_k \tag{89}$$

Likewise we can write

$$L_i \mathsf{Q}_i \equiv \textstyle\sum_j \overline{B}_{ij} \mathbf{t}_j \otimes \hat{\mathbf{t}}_j = \sum_{j,k} \frac{1}{2} \overline{B}_{ij} \mathbf{t}_j \otimes \hat{\mathbf{t}}_j \overline{A}_{jk}. \tag{90}$$

To leading order, strain gradients can be neglected and we may assume $\overline{C}_{ik}(\mathsf{E}_k - \mathsf{E}_i) = \mathsf{0}$. Then the symmetric force stress over a tristar is given by

$$\hat{E}_k \boldsymbol{\sigma}_k = \textstyle\sum_i \left[K_{ik} \mathcal{P}_i \mathsf{I} + \frac{1}{2} \mathcal{T}_i \sum_j \overline{B}_{ij} \mathbf{t}_j \otimes \hat{\mathbf{t}}_j \overline{A}_{jk} \right]. \tag{91}$$

Taking the trace gives the isotropic stress over a tristar as

$$P_{\mathrm{eff},k} = \sum_i \left[\frac{K_{ik} \mathcal{P}_i}{\hat{E}_k} + \frac{1}{4\hat{E}_k} \mathcal{T}_i \textstyle\sum_j \overline{B}_{ij} t_j \overline{A}_{jk} \right]. \tag{92}$$

The deviatoric stress is symmetric, and is

$$\boldsymbol{\sigma}_k^{(s)} = \frac{1}{2\hat{E}_k} \textstyle\sum_{i,j} \mathcal{T}_i \overline{B}_{ij} t_j (\hat{\mathbf{t}}_j \otimes \hat{\mathbf{t}}_j - \frac{1}{2}\mathsf{I}) \overline{A}_{jk}. \tag{93}$$

The micoscopic stress over the tristar is

$$\hat{E}_k \tilde{\boldsymbol{\sigma}}_k = \cup_i \left[K_{ik} \mathcal{P}_i \mathsf{I} + \tfrac{1}{2} \mathcal{T}_i \cup_j \overline{B}_{ij} \mathbf{t}_j \otimes \hat{\mathbf{t}}_j \overline{A}_{jk} \right]. \tag{94}$$

[*Show that* $\mathrm{div}^t \tilde{\boldsymbol{\sigma}}_k = \mathbf{0}$*, where* div^t *is a divergence over tristars rather than triangles. Break the integral into divergence over each kite, and recover force balance over vertex* k*.*]

[*Consider alternative formulations over triangles, rather than tristars.*]

In general, we do not expect $\mathrm{div}^v \boldsymbol{\sigma}_k$ to vanish, whether or not it is defined over triangles or tristars.

References

[1] T. Nagai and H. Honda. A dynamic cell model for the formation of epithelial tissues. *Phil. Mag. B*, 81:699–719, 2001.

[2] R. Farhadifar, J.-C. Röper, B. Aigouy, S. Eaton, and F. Jülicher. The influence of cell mechanics, cell-cell interactions, and proliferation on epithelial packing. *Curr. Biol.*, 17:2095–2104, 2007.

[3] D. B. Staple, R. Farhadifar, J. C. Roeper, B. Aigouy, S. Eaton, and F. Jülicher. Mechanics and remodelling of cell packings in epithelia. *Eur. Phys. J. E*, 33:117–127, 2010.

[4] A. G. Fletcher, M. Osterfield, R. E. Baker, and S. Y. Shvartsman. Vertex models of epithelial morphogenesis. *Biophys. J.*, 106:2291–2304, 2014.

[5] S. Alt, P. Ganguly, and G. Salbreux. Vertex models: from cell mechanics to tissue morphogenesis. *Phil. Trans. R. Soc. B*, 372(1720):20150520, 2017.

[6] S. Ishihara and K. Sugimura. Bayesian inference of force dynamics during morphogenesis. *J. Theor. Biol.*, 313:201–211, 2012.

[7] X. Yang, D. Bi, M. Czajkowski, M. Merkel, M. L. Manning, and M. C. Marchetti. Correlating cell shape and cellular stress in motile confluent tissues. *Proc. Nat. Acad. Sci.*, 114(48):12663–12668, 2017.

[8] A. Nestor-Bergmann, G. Goddard, S. Woolner, and O. E. Jensen. Relating cell shape and mechanical stress in a spatially disordered epithelium using a vertex-based model. *Math. Med. Biol.*, 35:1–27, 2018.

[9] A. Nestor-Bergmann, E. Johns, S. Woolner, and O. E. Jensen. Mechanical characterization of disordered and anisotropic cellular monolayers. *Phys. Rev. E*, 97:052409, May 2018.

[10] S. Tong, N. K. Singh, R. Sknepnek, and A. Kosmrlj. Linear viscoelastic properties of the vertex model for epithelial tissues. *arXiv preprint arXiv:2102.11181*, 2021.

[11] T. Higashi and A. L. Miller. Tricellular junctions: how to build junctions at the TRICkiest points of epithelial cells. *Molecular biology of the cell*, 28(15):2023–2034, 2017.

[12] F. Bosveld, Z. Wang, and Y. Bellaïche. Tricellular junctions: a hot corner of epithelial biology. *Current opinion in cell biology*, 54:80–88, 2018.

[13] A. Nestor-Bergmann, G. A. Stooke-Vaughan, G. K. Goddard, T. Starborg, O. E. Jensen, and S. Woolner. Decoupling the roles of cell shape and mechanical stress in orienting and cueing epithelial mitosis. *Cell Reports*, 26(8):2088–2100, 2019.

[14] A. Angulo-Urarte, T. van der Wal, and S. Huveneers. Cell-cell junctions as sensors and transducers of mechanical forces. *Biochimica et Biophysica Acta (BBA)-Biomembranes*, 1862(9):183316, 2020.

[15] H. H. Yu and J. A. Zallen. Abl and Canoe/Afadin mediate mechanotransduction at tricellular junctions. *Science*, 370(6520):eaba5528, 2020.

[16] P. Howell, G. Kozyreff, and J. Ockendon. *Applied solid mechanics*. Cambridge University Press, 2009.

[17] O. E. Jensen, E. Johns, and S. Woolner. Force networks, torque balance and Airy stress in the planar vertex model of a confluent epithelium. *Proc. Roy. Soc. A*, 2020.

[18] L. J. Grady and J. R. Polimeni. *Discrete calculus: Applied analysis on graphs for computational science*. Springer Science & Business Media, 2010.

[19] R. D. Mindlin. Influence of couple-stresses on stress concentrations. Technical report, Columbia University, New York, 1962.

[20] A. R. Hadjesfandiari and G. F. Dargush. Couple stress theory for solids. *Int. J. Solids & Struct.*, 48(18):2496–2510, 2011.

[21] L. B. da Veiga, K. Lipnikov, and G. Manzini. *The mimetic finite difference method for elliptic problems*, volume 11. Springer, 2014.

[22] Dapeng Bi, Silke Henkes, Karen E Daniels, and Bulbul Chakraborty. The statistical physics of athermal materials. *Annu. Rev. Condens. Matter Phys.*, 6(1):63–83, 2015.

[23] L. Yan and D. Bi. Multicellular rosettes drive fluid-solid transition in epithelial tissues. *Phys. Rev. X*, 9(1):011029, 2019.

[24] K. Ramola and B. Chakraborty. Stress response of granular systems. *J. Stat. Phys.*, 169(1):1–17, 2017.

[25] L. E. Edens, E. G. Alvarado, A. Singh, J. F. Morris, G. K. Schenter, J. Chun, and A. E. Clark. Shear stress dependence of force networks in 3d dense suspensions. *Soft Matter*, 17(32):7476–7486, 2021.

[26] A. Mann, R. S. Sopher, S. Goren, O. Shelah, O. Tchaicheeyan, and A. Lesman. Force chains in cell–cell mechanical communication. *J. Roy. Soc. Interface*, 16(159):20190348, 2019.

[27] S. Kim, M. Pochitaloff, G. A. Stooke-Vaughan, and O. Campàs. Embryonic tissues as active foams. *Nature Phys.*, 17(7):859–866, 2021.

[28] A. Nestor-Bergmann, G. B. Blanchard, N. Hervieux, A. G. Fletcher, J. Étienne, and B. Sanson. Adhesion-regulated junction slippage controls cell intercalation dynamics in an apposed-cortex adhesion model. *PLOS Comp. Biol.*, 18(1):e1009812, 2022.

[29] M. Weliky and G. Oster. The mechanical basis of cell rearrangement. I. Epithelial morphogenesis during Fundulus epiboly. *Development*, 109(2):373–386, 1990.

[30] T. Yamamoto, T. Hiraiwa, and T. Shibata. Collective cell migration of epithelial cells driven by chiral torque generation. *Phys. Rev. Research*, 2(4):043326, 2020.

[31] M. Desbrun, A. N. Hirani, M. Leok, and J. E. Marsden. Discrete exterior calculus. *arXiv preprint math/0508341*, 2005.

[32] K. Lipnikov, G. Manzini, and M. Shashkov. Mimetic finite difference method. *J. Comp. Phys.*, 257:1163–1227, 2014.

[33] L.-H. Lim. Hodge Laplacians on graphs. *SIAM Review*, 62(3):685–715, 2020.